J. Fluid Mech. (2019), *vol.* 862, *pp.* 128–161.
doi:10.1017/jfm.2018.941

The role of gravity in the prediction of the circular hydraulic jump radius for high-viscosity liquids

Yunpeng Wang[1] **and Roger E. Khayat**[1,†]

[1]Department of Mechanical and Materials Engineering, University of Western Ontario, London, Ontario, Canada N6A 5B9

(Received 12 May 2018; revised 24 August 2018; accepted 20 November 2018; first published online 7 January 2019)

The free-surface flow formed by a circular jet impinging on a stationary disk is analysed theoretically. We develop a simple and coherent model to predict the location and height of the jump for high-viscosity liquids. The study explores the effect of gravity in the supercritical flow. The formulation reduces to a problem, involving only one parameter: $\alpha = Re^{1/3}Fr^2$, where Re and Fr are the Reynolds and Froude numbers based on the flow rate and the jet radius. We show that the jump location coincides with the singularity in the thin-film equation when gravity is included, suggesting that the jump location can be determined without the knowledge of downstream flow conditions such as the jump height, the radius of the disk, which corroborates earlier observations in the case of type I circular hydraulic jumps. Consequently, there is no need for a boundary condition downstream to determine the jump radius. Our results corroborate well existing measurements and numerical simulation. Our predictions also confirm the constancy of the Froude number Fr_J based on the jump radius and height as suggested by the measurements of Duchesne *et al.* (*Europhys. Lett.*, vol. 107, 2014, 54002). We establish theoretically the conditions for Fr_J to remain independent of the flow rate. The subcritical flow and the height of the hydraulic jump are sought subject to the thickness at the edge of the disk, comprising contributions based on the capillary length and minimum flow energy. The thickness at the edge of the disk appears to be negligibly small for high-viscosity liquids.

Key words: boundary layers, interfacial flows (free surface), thin films

1. Introduction

We examine the thin-film flow as a result of a circular jet impinging on a stationary disk. A circular hydraulic jump is expected to arise when a fluid jet falling vertically at high Reynolds number impacts the disk. The fluid spreads radially as a thin film until reaching a critical radius at which the film rises abruptly. Although the impingement of a circular jet has been extensively considered, there remain important

† Email address for correspondence: rkhayat@uwo.ca

issues as to a fully predictive theoretical formulation, particularly concerning the prediction of the jump location and height. Early predictions for the jump radius based on inviscid theory were reported by Rayleigh (1914), which did not yield a good agreement with experiment (Watson 1964). Although Tani (1949) considered viscous effects later, the dominant influence of viscosity was addressed much later. In fact, Watson (1964) formulated an appropriate description of the developing boundary layer and the fully viscous layer upstream of the jump. Watson (1964) studied both the radial and planar jet spreads for steady laminar and turbulent flows. Watson's thin-film approach became the basis for numerous theoretical and experimental studies. The jump location is of major fundamental significance, and its prediction remains somewhat incomplete, as far as a coherent and simple theory is concerned, despite the various existing theoretical and numerical approaches in the literature. It will be a major focus in the present study. In particular, we explore the role of gravity and its influence on the location of the jump. We demonstrate the crucial role of gravity for liquids of relatively large viscosity and low surface tension. The influence of surface tension was the focus of the recent study of Bhagat *et al.* (2018).

Numerous existing studies follow essentially the same approach as proposed by Watson (1964), where the flow domain comprises a developing boundary layer followed by a supercritical viscous film layer ahead of the jump and a subcritical layer downstream of the jump. This description appears to mimic well the flow for a type I hydraulic jump, where the jump is relatively abrupt, followed by flow separation and the emergence of a vortex downstream. Upstream of the jump, the location where the boundary layer reaches the free surface separates the developing boundary-layer region from the fully viscous region. The boundary-layer height before this transition point is typically determined using a Kármán–Pohlhausen approach and the similarity profile for the velocity. Downstream of the transition point, the same similarity profile is assumed to (approximately) hold. Based on the balance of forces, a relation between the jump location and the height is also obtained for both laminar and turbulent flows. Watson's theory was tested in a number of experimental investigations, including those of Watson himself, Craik *et al.* (1981), Stevens & Webb (1992), Bush & Aristoff (2003) and Baonga, Gualous & Imbert (2006). Liu & Lienhard (1993) observed that Watson's predictions are least satisfactory in the limit of relatively weak jump. Surface tension effect was neglected in Watson's work, and was later included by Bush and co-workers for a small circular jump radius, which led to a better agreement with experiment. They elucidated the influence of surface tension on the circular hydraulic jump, on both its size (Bush & Aristoff 2003) and its stability (Bush, Aristoff & Hosoi 2006) through combined theoretical and experimental investigations. The instability and the transition to polygonal hydraulic jump were originally reported by Ellegaard *et al.* (1998, 1999). The transition to type II and polygonal jump will not be considered here.

Watson's theory is generally considered to be adequate for a circular jump with relatively large radius and height. Some extensions have been considered, such as the spread of an impinging non-Newtonian jet by Zhao & Khayat (2008), the formation of hydraulic jump on an inclined plane by Kate, Das & Chakraborty (2007) and Benilov (2015), and the impingement on a rotating disk by Ozar, Cetegen & Faghri (2003) and Wang & Khayat (2018). The influence of slip was also examined by Dressaire *et al.* (2010), Prince, Maynes & Crockett (2012) and Khayat (2016). Another extension involves the influence of gravity on the jump radius (Avedisian & Zhao 2000).

The fully theoretical prediction of the simultaneous location and height of the jump remains lacking in typical analyses. We recall that Watson's approach and similar formulations provide only one relation between the jump radius and height in the form of an averaged momentum equation discretized across the jump. A second relation is therefore required. Moreover, the location of the jump is not always identifiable in reality, especially for high-viscosity liquids and flow at low rate. Avedisian & Zhao (2000) published photographs of the transition across the jump from submerged views, which illustrate the difficulty in identifying the jump location when the height changes gradually as result of a sudden reduction of gravity. The numerical simulation of Rojas, Argentina & Tirapegui (2010) also depicts the ambiguity in the jump location. Their numerical film profiles in their figure 2 illustrate how the abrupt jump ceases to exist with increasing viscosity, giving way to a smoother profile.

The full prediction of the jump location has been the focus of several studies. Following the approach of Tani (1949), Bohr, Dimon & Putzkaradze (1993) obtained the shallow-water equations for the average radial velocity and fluid depth by averaging the axisymmetric Navier–Stokes equations and in the vertical direction. They eliminated the depth from the averaged mass and momentum equations, and derived an ordinary differential equation for the average velocity. The equation turned out to have a single critical point which is a spiral (see Tani (1949)), and can exhibit an essential singularity at some finite distance. Bohr *et al.* (1993) argued that the jump location is close to the critical spiral point of their averaged equation, and deduced that the jump radius scales as $Q^{5/8}\nu^{-3/8}g^{-1/8}$, where Q is the jet flow rate, ν is the kinematic viscosity and g is the acceleration due to gravity. They also identified the location of the disk edge where the singularity occurs. The influence of the flow rate, the viscosity and the nozzle-to-disk distance on the hydraulic jump radius was investigated experimentally by Brechet & Neda (1999), who reached a scaling law similar to that proposed by Bohr *et al.* (1993). They also observed that the nozzle-to-disk distance has no influence on the jump location. Kasimov (2008) modified the formulation of Bohr *et al.* (1993) by adding the effect of surface tension and incorporating the shape of a flat plate with a falling edge. He studied the influence of surface tension on the stability of the hydraulic jump, and found that a steady jump may not exist at high surface tension. In a later work, Bohr, Putkaradze & Watanabe (1997) and Watanabe, Putkaradze & Bohr (2003) adopted a non-self-similar cubic profile for the velocity that allowed them to avoid the critical point and the singularity of the averaged equations. However, two experimental points are needed in their solution to fix the boundary conditions, and some prior knowledge of the location of the jump was required. We shall refer back to the contributions of Bohr and associates later in this study.

Additional studies of numerical nature were also done. Passandideh-Fard, Teymourtash & Khavari (2011) proposed a numerical approach to determine the hydraulic jump location. The free surface was tracked by a volume-of-fluid approach. In their calculation domain, the downstream depth was imposed at the disk edge. Rojas *et al.* (2010), Rojas, Argentina & Tirapegui (2013), Rojas & Tirapegui (2015) developed and implemented a spectral representation for the velocity profile in the vertical direction. The projected averaged dynamical system is multidimensional in this case. More details on the work of Rojas and associates will be given when we compare our predictions with theirs.

Duchesne, Lebon & Limat (2014) showed experimentally that the Froude number based on the jump height and velocity is independent of the flow rate, the viscosity and the surface tension. This critical Froude number, denoted here by Fr_J, is therefore

a constant, and should in principle provide the desired additional relation, which when coupled with Watson's discretized momentum relation, would allow the full prediction of the jump location and height. However, no theoretical justification was provided. More recently, the measurements of Mohajer & Li (2015) do indeed support the claim of Duchesne *et al.* (2014), but found that the Froude number is not independent of the surface tension. Recently, Wang & Khayat (2018) revisited this issue in their study of the flow on a rotating disk, and provided some theoretical arguments and comparison with experiment in support of the claim of Duchesne *et al.* (2014). The thickness at the edge of the disk was determined as a combination of static and dynamic contributions based on the local minimization of energy. The Froude number was found to remain essentially independent of the flow rate. However, the predictions were limited to low-viscosity liquids and high flow rates.

This brings us to the main objective of the present study, focused on the theoretical prediction of the jump location and height for liquids of high viscosity. In this case, gravity becomes important for the supercritical flow. We therefore explore the interplay among inertia, viscosity and gravity for a thin film flowing axisymmetrically on a stationary disk as a result of jet impingement. In § 2, we outline the problem by giving the governing equations and boundary conditions in each region of the physical domain. The overall solution strategy is also discussed. In § 3, the Kármán–Pohlhausen (KP) approach is adopted to determine the boundary-layer structure and the film thickness upstream of the jump. The transition point is also located, where the boundary-layer edge and the free surface meet. In § 4, the KP approach is employed again to examine the viscous boundary-layer region, and assess the influence of gravity on the thin-film flow and jump location. Comparison with experiment is also carried out. In § 5, the height of the hydraulic jump is determined using a momentum balance across the jump, and the effect of gravity on the jump is analysed. The drawback of this approach is discussed. Alternatively, we propose an approach based on the knowledge of the edge thickness, which is established following the recent study of Wang & Khayat (2018). Finally, concluding remarks and discussion are given in § 6.

2. Physical domain and problem statement

Consider the steady laminar incompressible flow of a circular (axisymmetric) jet of a Newtonian fluid emerging from a nozzle of radius a, impinging at a volume flow rate Q on a flat disk lying normal to the jet direction. The flow configuration is depicted schematically in figure 1, where dimensionless variables and parameters are used. The problem is formulated in the (r, θ, z) fixed coordinates, with the origin coinciding with the disk centre. The flow is assumed to be independent of θ, thus excluding polygonal flow. In this case, $u(r, z)$ and $w(r, z)$ are the corresponding dimensionless velocity components in the radial and vertical directions, respectively. The r-axis is taken along the disk radius and the z-axis is taken parallel to the jet. The length and the velocity scales are conveniently taken to be the radius of the jet, a, and $Q/\pi a^2$ both in the radial and vertical directions. Since the pressure is expected to be predominantly hydrostatic for a thin film, it will be scaled by $\rho g a$. Two main dimensionless groups emerge in this case: the Reynolds number $Re = Q/\pi a\nu$, where ν is the kinematic viscosity, and the Froude number $Fr = Q/\pi\sqrt{a^5 g}$, g being the acceleration due to gravity. We shall see that the problem can be reduced to a one-parameter problem, but the two parameters remain useful when comparing with experiment.

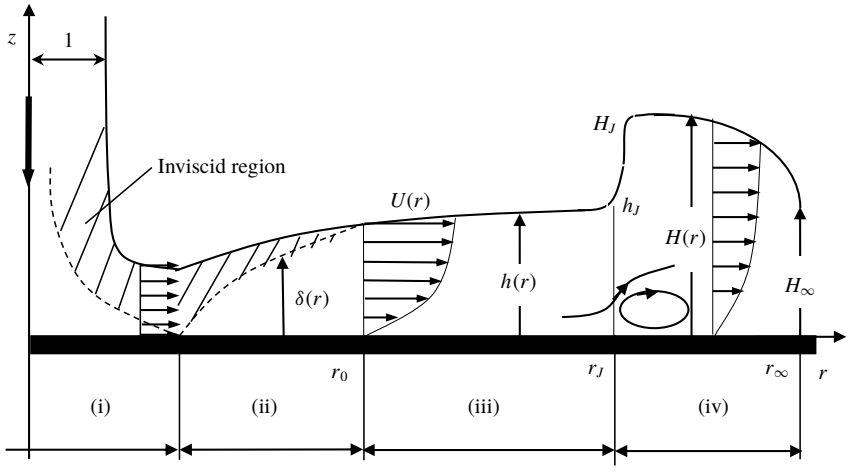

FIGURE 1. Schematic illustration of the axisymmetric jet flow impinging on a flat stationary disk and the hydraulic jump of type I with one vortex downstream. Shown are the stagnation region (i), the developing boundary-layer region (ii), the fully developed viscous region (iii) and the hydraulic jump region (iv). All notations are dimensionless.

2.1. *The physical domain*

Following the treatment of Watson (1964), we identify four distinct flow regions for the jet over a circular disk, with smooth passage from one region to the next (see figure 1): a stagnation flow region (i), a developing boundary-layer region (ii), where the boundary layer grows until it reaches the film surface at the transition location $r = r_0$ and a fully viscous thin-film region (iii). A hydraulic jump emerges in region (iv), located at a radius $r = r_J$. We observe that $r = O(1)$ near the stagnation point in region (i). The velocity outside the boundary layer rises rapidly from 0 at the stagnation point to the impingement velocity in the inviscid far region. In region (ii), and as we shall confirm, the boundary layer is not expected to grow like $\sqrt{r/Re}$ in the presence of gravity. The speed outside the boundary layer remains almost constant, as the fluid here is unaffected by the viscous stresses. For $r \gg 1$, the flow field in region (ii) is not significantly affected by the stagnation flow of region (i). The region $1 \ll r < r_0$ will be referred to as the developing boundary-layer region, with boundary-layer thickness $\delta(r)$, outside which the flow is inviscid and uniform. Here r_0 is the location of the transition point at which the viscous stresses become appreciable right up to the free surface, where the whole flow is of the boundary-layer type. At this point, in the absence of gravity, the velocity profile changes from the Blasius type to the self-similar profile. In contrast, in the presence of gravity, a similarity profile does not exist. The flow in region (iii), $r > r_0$, which will be referred to as the fully developed viscous region, is bounded by the disk and the free surface $z = h(r)$.

Finally, the hydraulic jump in region (iv) occurs at a location $r = r_J$, which is larger than r_0 since the jump typically occurs downstream of the transition point. Referring to figure 1, we conveniently introduce the supercritical film thickness (upstream of the jump) as $h(r) = h(r < r_J)$, and the subcritical thickness (downstream of the jump) as $H(r) \equiv h(r > r_J)$. The height immediately upstream of the jump is denoted by $h_J \equiv h(r = r_J)$, and the height immediately downstream of the jump is denoted by $H_J \equiv H(r = r_J)$. The subcritical height $H(r)$ is generally not constant and is different from

the height H_J. In this study, the fluid is assumed to be drained at the edge of the disk, at $r = r_\infty$, and the flow remains steady, with the film thickness denoted by $H_\infty = H(r = r_\infty)$. Although it is common practice to assume the jump height to remain equal to H_J, this assumption is valid for fluids of low viscosity. The edge thickness is not expected to depend heavily on the flow rate (Rojas *et al.* 2013; Mohajer & Li 2015).

2.2. *Governing equations and boundary conditions*

Unless otherwise specified, the Reynolds number is assumed to be moderately large so that our analysis is confined to the laminar regime. Consequently, for steady axisymmetric thin-film flow, in the presence of gravity, the mass and momentum conservation equations are formulated using a thin-film or Prandtl boundary-layer approach, which amounts to assuming that the radial flow varies much slower than the vertical flow (Schlichtling 2000). By letting a subscript with respect to r or z denote partial differentiation, the reduced dimensionless conservation equations become

$$u_r + \frac{u}{r} + w_z = 0, \tag{2.1a}$$

$$Re(uu_r + wu_z) = -\frac{Re}{Fr^2}p_r + u_{zz}, \tag{2.1b}$$

$$p_z = -1. \tag{2.1c}$$

Here, p is the dimensionless pressure.

These are the thin-film equations commonly used to model the spreading liquid flow (Tani 1949; Bohr *et al.* 1993, 1996; Kasimov 2008). We observe that the pressure for a thin film is hydrostatic as a result of its vanishing at the film surface (in the absence of surface tension) and the small thickness of the film. In addition, upstream of the jump, the variation of the film thickness with the radius is expected to be smooth and gradual. In this case, the radial variation of the hydrostatic pressure is also small. Unlike the case of liquids of low viscosity, gravity cannot be neglected in the supercritical range. At the disk, the no-slip and no-penetration conditions are assumed to hold for any r. In this case:

$$u(r, z = 0) = w(r, z = 0) = 0. \tag{2.2}$$

At the free surface $z = h(r < r_J)$ or $z = H(r > r_J)$, the kinematic and dynamic conditions for steady flow take the form

$$w(r, z = h) = u(r, z = h)h'(r), \quad u_z(r, z = h) = p(r, z = h) = 0. \tag{2.3a,b}$$

Here a prime denotes total differentiation. The flow field is sought separately in the developing boundary-layer region (ii) for $0 < r < r_0$, the fully developed viscous boundary-layer region (iii) for $r_0 < r < r_J$ and the hydraulic jump region (iv) for $r_J < r < r_\infty$. We observe that region (i) is neglected and will not be considered here. In this case, the leading edge of the boundary layer in region (ii) is taken to coincide with the disk centre. Consequently, the additional boundary conditions are as follows. In region (ii), the flow is assumed to be sufficiently inertial for inviscid flow to prevail between the boundary-layer outer edge and the free surface (see figure 1). In this case, the following conditions at the outer edge of the boundary layer and beyond must hold:

$$u_z(r < r_0, z = \delta) = 0, \quad u(r < r_0, \delta \leqslant z < h) = 1. \tag{2.4a,b}$$

Integrating (2.1*c*) subject to condition (2.3*b*), the pressure becomes $p(r, z) = h(r) - z$, which is then eliminated so that (2.1*b*) reduces to

$$Re(uu_r + wu_z) = -\frac{Re}{Fr^2}h' + u_{zz}. \tag{2.5}$$

Finally, the conservation of mass at any location upstream and downstream of the jump yields the following relation in dimensionless form:

$$\frac{1}{2r} = \int_0^{h(r)} u(r < r_j, z)\,\mathrm{d}z = \int_0^{H(r)} u(r > r_j, z)\,\mathrm{d}z. \tag{2.6}$$

The presence of gravity causes the flow to be non-self-similar in character. Therefore, in the present study, approximate solutions are sought in each region. An integral approach of the Kármán–Pohlhausen (KP) type (Schlichtling 2000) is adopted upstream of the jump, similar to the formulation of Prince *et al.* (2012) for a jet impinging on a disk with slip. The cubic profile is used for the velocity, which is considered to be the leading-order solution in a comprehensive spectral approach when inertia is included (Khayat & Kim 2006; Rojas *et al.* 2010). The cubic profile seems to be amply adequate as it leads to close agreement with Watson's (1964) similarity solution for a jet impinging on a stationary disk (Prince *et al.* 2012). The cubic profile was also assessed by Khayat (2016) for a planar jet impinging on a surface with slip, and was found to yield a good agreement against his numerical solution. See also Rao & Arakeri (1998) for an integral analysis of a rotating film. Higher-order polynomial velocity profiles were also used. In their study on flow separation and wave breaking, Bohr *et al.* (1996) used a quartic profile to illustrate the emergence of a singularity at the separation point for a thin film. The coefficients in the polynomial expansion were not obtained explicitly. A cubic velocity profile was later adopted by Bohr *et al.* (1997), accounting for regions of separation. The cubic profile was also adopted in our recent study for a jet impinging on a rotating disk (Wang & Khayat 2018), and was found to yield close agreement with experiment.

3. The flow in the developing boundary layer and the transition location

Throughout this study, the stagnation region (i) under the impinging jet will not be considered. The velocity outside the boundary layer rises rapidly from 0 at the stagnation point to the impingement velocity in the inviscid far region. The impinging jet is predominantly inviscid close to the stagnation point, and the boundary-layer thickness remains negligibly small. Obviously, this is the case for a jet at relatively large Reynolds number. Ideally, the flow at the boundary-layer edge should correspond to the (almost parabolic) potential flow near the stagnating jet, with the boundary-layer leading edge coinciding with the stagnation point (Liu, Gabour & Lienhard 1993). However, the assumption of uniform horizontal flow near the wall and outside the boundary layer (as illustrated in figure 1) is reasonable. The distance from the stagnation point for the inviscid flow to reach uniform horizontal velocity is small, of the order of the jet radius (Lienhard 2006). In the absence of gravity, the flow acquires a similarity character. In this case, the position or effect of the leading edge is irrelevant. This is not the case in the presence of gravity, where, as we shall see, a non-self-similar solution should be sought subject to initial conditions at the leading edge. However, the dominance of inertia near the stagnation point, albeit weakened by gravity, should make plausible the assumption of uniform horizontal flow.

This assumption was adopted initially by Watson (1964), and is commonly used in the existing theories (see, for instance, Higuera (1994), Bush & Aristoff (2003), Prince *et al.* (2012)).

We therefore start by examining the flow in region (ii), where the inviscid flow dominates the upper layer ($\delta \leqslant z < h$) of the film in the radial direction. Consequently, the radial velocity above the boundary layer remains equal to one: $U(r) = 1$. The boundary-layer height δ is determined by considering the mass and momentum balance over the boundary-layer region (ii). Therefore, we consider first the integral form of the convective term in (2.5). The vertical velocity component is eliminated by noting from (2.1*a*) that $w(r, z) = -(1/r)(\partial/\partial r)(r \int_0^z u(r, z)\,\mathrm{d}z)$. In this case,

$$uu_r + wu_z = \frac{\partial u^2}{\partial r} + \frac{u^2}{r} - \frac{1}{r}\frac{\partial}{\partial z}\left(u(r, z)\int_0^z \frac{\partial ru(r, \bar{z})}{\partial r}\mathrm{d}\bar{z}\right). \tag{3.1}$$

Consequently, upon integrating (3.1) across the boundary-layer thickness, we obtain the integral form of the momentum equation in the boundary-layer region:

$$\frac{Re}{r}\left[\frac{\mathrm{d}}{\mathrm{d}r}\int_0^\delta ru(u-1)\,\mathrm{d}z\right] = -\frac{Re}{Fr^2}h'\delta - u_z(r, z=0). \tag{3.2}$$

The boundary layer grows with radial distance, eventually invading the entire film width, reaching the jet free surface at $r = r_0$. For $r < r_0$ and above the boundary-layer outer edge, at some height $z = h(r) > \delta(r)$, lies the free surface. The height of the free surface in region (ii) is then determined from mass conservation inside and outside the boundary layer. Therefore, for $r < r_0$,

$$\int_0^{\delta(r)} u(r, z)\,\mathrm{d}z + h(r) - \delta(r) = \frac{1}{2r}. \tag{3.3}$$

For simplicity, we choose a cubic profile for the velocity. Thus, we let

$$u(r < r_0, z) = \frac{3}{2}\left(\frac{z}{\delta}\right) - \frac{1}{2}\left(\frac{z}{\delta}\right)^3 = \frac{1}{2}\eta(3-\eta^2) \equiv f(\eta), \tag{3.4}$$

where $\eta = z/\delta$. The cubic profile (3.4) is obviously one of many that can be used. The cubic profile, which will also be modified and implemented in the fully viscous region (iii), does not satisfy the momentum equation at $z = 0$ except in the absence of a pressure gradient. But so do many profiles used in the literature, including the parabolic profile used by Bohr *et al.* (1993) and Kasimov (2008). The inclusion of the pressure gradient yields a non-self-similar profile, making the problem mathematically more cumbersome. For this reason, simple profiles are often adopted in the literature, including the cubic profile used by Prince *et al.* for a flow on a disk with isotropic (2012) and anisotropic (2014) slip, Watson's (axisymmetric) similarity profile used by Dressaire *et al.* (2010) to simulate non-axisymmetric hydraulic jump patterns. None of these profiles satisfy the momentum equation at the disk, yet they all lead to an accurate description. See, for instance, the comparisons of Dressaire *et al.* (2010), Prince *et al.* (2012) and Khayat (2016). The profile (3.4) fulfils desirable criteria as it is simple and, and as we shall see, yields accurate results.

Upon inserting (3.4) into (3.2) and (3.3), we obtain the following coupled equations for the boundary-layer and free-surface heights:

$$h - \frac{3}{8}\delta = \frac{1}{2r}, \tag{3.5*a*}$$

$$\frac{39}{280}\frac{Re}{r}\delta\frac{\mathrm{d}}{\mathrm{d}r}(r\delta)=\frac{Re}{Fr^2}h'\delta^2+\frac{3}{2}. \tag{3.5b}$$

These equations are solved subject to $\delta(r=0)=0$. In the absence of gravity ($Fr\to\infty$), equations (3.5) are easily solved to yield the following boundary-layer and film thicknesses:

$$\delta(r<r_0)=2\sqrt{\frac{70}{39}\frac{r}{Re}},\quad h(r<r_0)=\frac{1}{4}\left(\frac{2}{r}+\sqrt{\frac{210}{13}\frac{r}{Re}}\right), \tag{3.6a,b}$$

which agree with the $\delta\approx\sqrt{r/Re}$ behaviour established from the dimensional argument of (2.5). In this case, h decreases rapidly, like $1/r$, near the disk centre, reaching a minimum, and increases like $\sqrt{r}$ further downstream. The transition location is determined by equating $h(r_0)$ and $\delta(r_0)$ to obtain $r_0=((78/875)Re)^{1/3}$.

In the presence of gravity, the system (3.5) must be solved numerically. The problem can be reduced to a one-parameter problem by introducing the following transformation:

$$r=Re^{1/3}\bar{r},\quad (h,\delta)=Re^{-1/3}(\bar{h},\bar{\delta}). \tag{3.7a,b}$$

Eliminating the film height and using (3.7), the equation for the boundary-layer height reduces to, along with the film thickness:

$$\frac{3}{4}\left(\frac{1}{\alpha}\bar{\delta}-\frac{13}{35}\right)\bar{\delta}\bar{\delta}'=\frac{39}{140}\left(\frac{\bar{\delta}^2}{\bar{r}}\right)+\frac{1}{\alpha}\frac{\bar{\delta}^2}{\bar{r}^2}-3,\quad \bar{h}=\frac{3}{8}\bar{\delta}+\frac{1}{2\bar{r}}. \tag{3.8a,b}$$

Here, we introduced

$$\alpha\equiv Re^{1/3}Fr^2, \tag{3.9}$$

which becomes the only parameter in the problem. Equation (3.8*a*) is solved numerically subject to $\bar{\delta}(\bar{r}=0)=0$, yielding in turn the height from (3.8*b*).

Figure 2 illustrates the influence of gravity on the boundary-layer height. In the limit of infinite Froude number, the classical boundary-layer result is recovered (Watson 1964; Schlichtling 2000). As expected, gravity can have a tangible effect as the profiles in figure 2 show a departure from the classical parabolic character of the boundary layer height. In fact, it is not difficult to show that the asymptotic solution of equation (3.8*a*) for small r that the behaviour of the boundary-layer height near impingement is linear with distance. More precisely, $\bar{\delta}=\sqrt{3\alpha}\bar{r}+O(\bar{r}^2)$, or $\delta\approx\sqrt{3}(Fr/\sqrt{Re})r$ as opposed to $\delta=2\sqrt{(70/39)r/Re}$ in the absence of gravity. The linear growth is clearly reflected by the $\alpha=10$ curve. Thus, the boundary-layer height approaches the linear behaviour with a diminishing slope as the level of gravity (or α) increases. We observe from (3.8*b*) that, since the boundary-layer height is small near the origin, the film height decays like $\bar{h}\sim 1/2\bar{r}$ regardless of the level of gravity. This behaviour is also reflected by the h curves in figure 2, showing a narrow spread when α is varied compared to δ. Gravity tends to lower the boundary-layer height.

The behaviour in figure 2 can also be deduced qualitatively from (2.5), where the effect of gravity tends to enhance the effect of inertia as a result of the decaying film thickness with distance. The level of inertia is reflected by the radial convective term $Re\,uu_r$. An estimate of the order of magnitude of this term is reached by taking

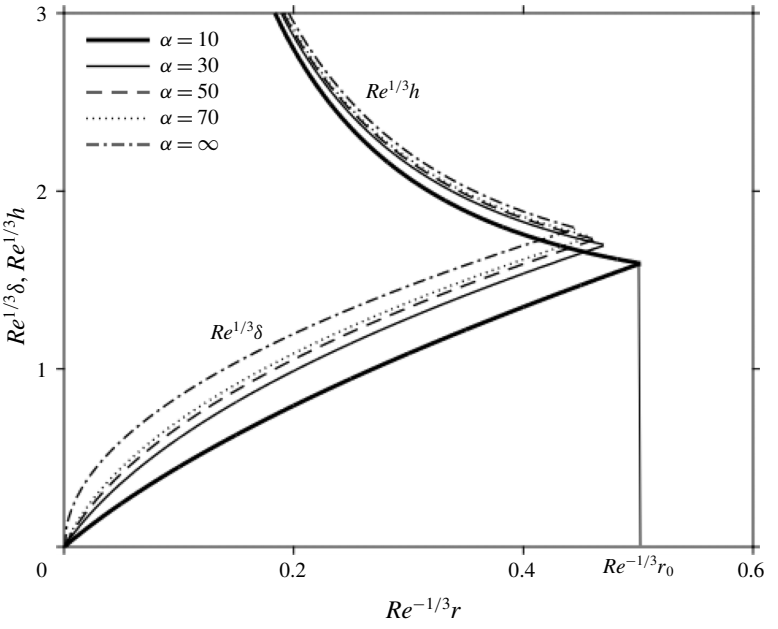

FIGURE 2. Influence of gravity in the developing boundary-layer region (ii). The rescaled boundary-layer height, δ, and film thickness, h, are plotted against the normalized radial distance. The transition location coincides with the intersection of the two heights (at the cusps in the figure). We only indicate the transition location by a vertical line for $\alpha = 10$.

u to correspond to the free-surface value. In this case, we see that $Re\, uu_r$ decays with distance like $Re\, r^{-1}$. There is an additional contribution to inertia stemming from gravity, namely through $-(Re/Fr^2)h' \sim (Re/2Fr^2)r^{-2}$ for small r, making the boundary-layer height behaves roughly like $\delta \sim \sqrt{r/Re}(1 + 1/2Fr^2 r)^{-1/2}$, which clearly shows the diminishing influence of gravity on the boundary-layer height. Thus, for dominant gravity, this relation reduces to $\delta \sim (Fr/Re)r$, which is the linear behaviour based on (3.8).

Figure 3 depicts the influence of gravity on the transition location r_0 and corresponding film thickness $h(r_0)$, which are determined by setting $h(r_0) = \delta(r_0)$. The transition location is further from impingement for a thinner film with increasing gravity effect as inertia is enhanced by gravity. This is the same trend predicted for the effect of slip (see figure 8 of Khayat (2016)). Similar to slip, gravity results in an asymptotic behaviour of the thickness for large α.

4. The fully viscous layer and prediction of the jump location

In this section, we formulate the problem for the film thickness in region (iii) and examine the flow field in this region. We then determine the location of the jump based on the supercritical flow without recourse to the subcritical solution. The approach is validated against existing measurements of the jump radius and its dependence on the flow rate.

4.1. *The equation for the film thickness*

In region (iii), the potential flow in the radial direction ceases to exist, with the velocity $U(r) = u(r, z = h)$ at the free surface becoming dependent on r. We again

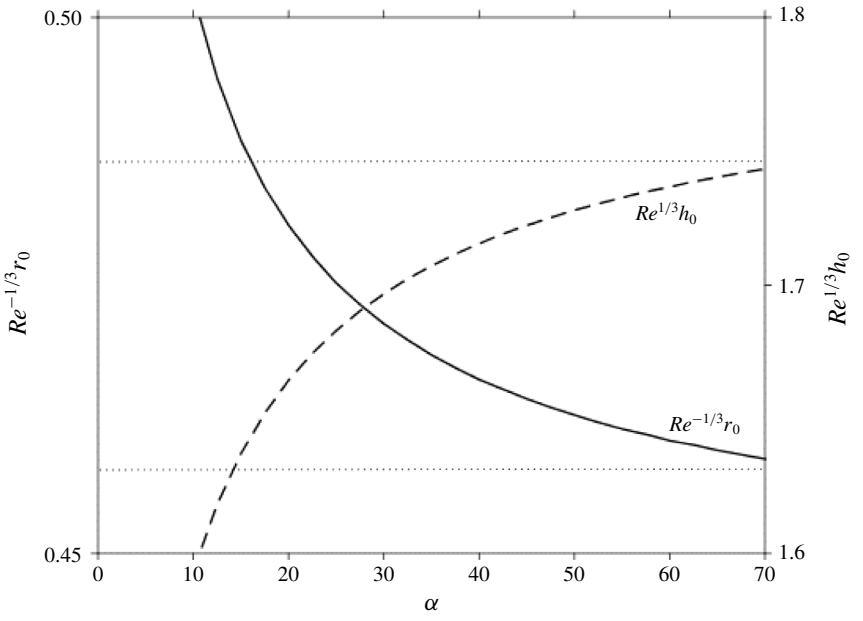

FIGURE 3. Dependence of the location and film thickness at the transition point between the developing and viscous boundary-layer regions (ii) and (iii) on gravity.

assume a cubic velocity profile subject to conditions (2.3*a*) and (2.3*b*). In this case, the radial velocity profile is given as function of the surface velocity $U(r)$ as

$$u(r_0 < r < r_J, z) = U(r)f(\eta), \quad \eta = \frac{z}{h(r)}. \tag{4.1a,b}$$

Here, we observe that $f(\eta)$ is still given by (3.4). Using the mass conservation (2.6) yields the following relation:

$$U(r_0 < r < r_J) = \frac{4}{5hr}. \tag{4.2}$$

This equation agrees with equation (15) of Prince *et al.* (2012) when setting their slip parameter equal to zero.

Similar to (3.2), the integral form of the momentum equation reads:

$$\frac{Re}{r}\frac{\mathrm{d}}{\mathrm{d}r}\int_0^h ru^2\,\mathrm{d}z = -\frac{Re}{Fr^2}hh' - u_z(r, z=0). \tag{4.3}$$

Substituting (4.1) into (4.3) and using (4.2) to eliminate U, we obtain the equation for the film thickness in the fully viscous region:

$$Re\left(\frac{1}{Fr^2} - \frac{272}{875r^2h^3}\right)h' = \frac{4}{5rh^2}\left(\frac{68Re}{175}\frac{1}{r^2} - \frac{3}{2h}\right), \tag{4.4}$$

which is solved for $r \geqslant r_0$ subject to $h(r = r_0) = \delta(r_0)$. We observe that the flow in the absence of gravity is recovered in the limit $Fr \to \infty$. In this case, the problem

reduces to the following equation and boundary condition:

$$\frac{\mathrm{d}h}{\mathrm{d}r} = -\frac{h}{r} + \frac{525}{136}\frac{r}{Re}, \quad h(r_0) = 2\sqrt{\frac{70}{39}\frac{r_0}{Re}}, \tag{4.5a,b}$$

which admits

$$h(r > r_0) = \frac{175}{136Rer}(r^3 - r_0^3) + 2\frac{r_0}{r}\sqrt{\frac{70}{39}\frac{r_0}{Re}} = \frac{175}{136}\frac{r^2}{Re} + \frac{233}{340}\frac{1}{r}, \tag{4.6}$$

as solution, where we recall $r_0 = ((78/875)Re)^{1/3}$. For comparison, Watson's expression is reproduced here in dimensionless form:

$$h(r > r_0) = \frac{2\pi}{3\sqrt{3}}\frac{r^2}{Re} + \frac{3c(3\sqrt{3}c - \pi)}{8\pi}\frac{1}{r}. \tag{4.7}$$

Thus, we have $h \approx 1.21(r^2/Re) + 0.685(1/r)$ from (4.6) compared to Watson's $h \approx 1.28(r^2/Re) + 0.69(1/r)$ from (4.7), showing a surprisingly close agreement, and validity of the cubic profile.

4.2. *The supercritical flow and the location of the hydraulic jump*

Equation (4.4) indicates that a singularity exists, occurring at some distance where the slope of the free surface becomes infinite. An equation similar to (4.4) was obtained by Bohr *et al.* (1993) by approximating the mean of the derivative of u^2 in the averaged momentum equation (4.3) in terms of the derivative of the mean square. They showed that the singularity is not an artefact of the averaging process, but is inherent to the thin-film equations. Of closer relevance is the equation obtained by Kasimov (2008) using a parabolic velocity profile, incorporating the shape of a finite disk with a sudden falling edge (see below).

We conjecture that the location of the singularity coincides with the radius of the jump. Consequently, we now have a relation between the jump radius r_J and the film height h_J immediately upstream of the jump:

$$Fr^{-2} = \frac{272}{875}\frac{1}{r_J^2 h_J^3}. \tag{4.8}$$

We therefore identify the jump location or radius to occur when the slope of the free surface upstream of the jump becomes infinite, that is $h'(r = r_J) \to \infty$, which coincides with the occurrence of the singularity of equation (4.4). At this location the relation between the jump radius and height is given by (4.8). Obviously, this claim is bold and needs to be validated, which we shall do shortly. The jump location is found by simply integrating (4.4) numerically subject to $h(r_0) = \delta(r_0)$ from r_0 to a distance r_J until (4.8) is satisfied to within a certain tolerance. More details on the numerical treatment are given below.

Before comparing the predicted jump radius with existing measurements, it is helpful to explore the general supercritical flow behaviour (upstream of the jump). Once again, the flow becomes governed by a one-parameter problem when transformation (3.7) is used. In this case, (4.4) reduces to

$$\left(\frac{1}{\alpha} - \frac{272}{875}\frac{1}{\bar{r}^2\bar{h}^3}\right)\bar{h}' = \frac{1}{\bar{r}\bar{h}^2}\left(\frac{272}{875}\frac{1}{\bar{r}^2} - \frac{6}{5\bar{h}}\right), \tag{4.9}$$

where we recall α from (3.9). In this case, relation (4.8) becomes

$$\bar{r}_J^2 \bar{h}_J^3 = \tfrac{272}{875}\alpha. \tag{4.10}$$

We observe that the velocity at the free surface remains invariant under transformation (3.7). Equation (4.9) is integrated numerically subject to the condition $\bar{h}(\bar{r}=\bar{r}_0) = \bar{\delta}(\bar{r}_0)$ at the transition point, using MATLAB sixth-order Runge–Kutta scheme. The integration is carried out at equal steps in the distance taken equal to 10^{-3}, until the turning point is reached at the singularity. The program is terminated when the slope $h' > 10^2$, giving an accuracy in the jump location r_J to the third decimal. The pre-jump height h_J is then deduced from (4.10).

We observe that equation (4.9), similar to equation (33) of Bohr *et al.* (1993) and equation (3.1)) of Kasimov (2008) for a flat disk, has only one critical point $\bar{h}_c = (6\alpha/5)^{1/4}$, $\bar{r}_c = \sqrt{272/875}(5/6)^{3/8}\alpha^{1/8}$, which is the root of the system $1/\alpha - (272/875)(1/\bar{r}^2\bar{h}^3) = (272/875)(1/\bar{r}^2) - 6/5\bar{h} = 0$, corresponding to a pair of complex conjugate eigenvalues of the Jacobian of the linearized two-dimensional dynamical system (Kasimov 2008). The real part is positive, indicating that the critical point is an unstable spiral, which in turn indicates that the solution cannot pass through the critical point. Bohr *et al.* (1993) estimated that the jump is located close to the critical point. They computed the flow and the free surface by choosing the pre-jump (inner) branch to correspond to a constant average velocity, and chose the post-jump (outer) branch that emanates from the point of singularity. The two branches are then joined by the shock when they reach the same radial position, at a point that is identified as the jump radius (see their figure 3). This method led them to deduce the scaling for the jump radius to be $R_J \approx Q^{5/8}\nu^{-3/8}g^{-1/8}$. In fact, if we assume the jump to occur at or near the critical point and recall (3.9), we obtain $\bar{r}_J \approx \bar{r}_c = \sqrt{272/875}(5/6)^{3/8}(Re^3Fr^2)^{1/8}$, which is the dimensionless form of the scaling deduced by Bohr *et al.* (1993).

Later, Kasimov (2008) derived an equation of closer similarity to (4.9) but introduced the shape of a flat disk with a cutoff at the edge. See his equation (3.1) and figure 2. The addition of the variable disk shape led to the existence of a critical saddle point near the disk edge, in addition to the spiral critical point. Kasimov determined the flow and the surface height on the two sides of the jump. The upstream branch is sought by solving his equation (3.1) subject to an initial condition corresponding the location where the jet velocity at impact equals the free-surface velocity. The downstream branch is sought by integrating (3.1) inward toward the jump starting at the far critical saddle point through which the solution effectively must pass. The integration is terminated on each side at the turning points, corresponding to an infinite slope in the surface height or the singularity in (3.1). The two heights computed on either side are subsequently used to determine the location of the jump by applying the discretized momentum equation.

Figure 4 gives an overview of the influence of gravity on the film thickness distribution up to the jump location. The film thickness exhibits a minimum typically downstream of the transition location. In general, gravity does not seem to have much of an effect until the jump is reached. In particular, and as expected by inspecting (2.5), near the minimum, gravity has a negligible effect. The jump occurs sooner and closer to transition point for a flow with stronger gravity.

The influence of gravity on the corresponding free-surface velocity profiles is depicted in figure 5. Here the velocity in the developing boundary-layer region (ii) outside the boundary layer is equal to 1 (the uniform jet velocity), which then

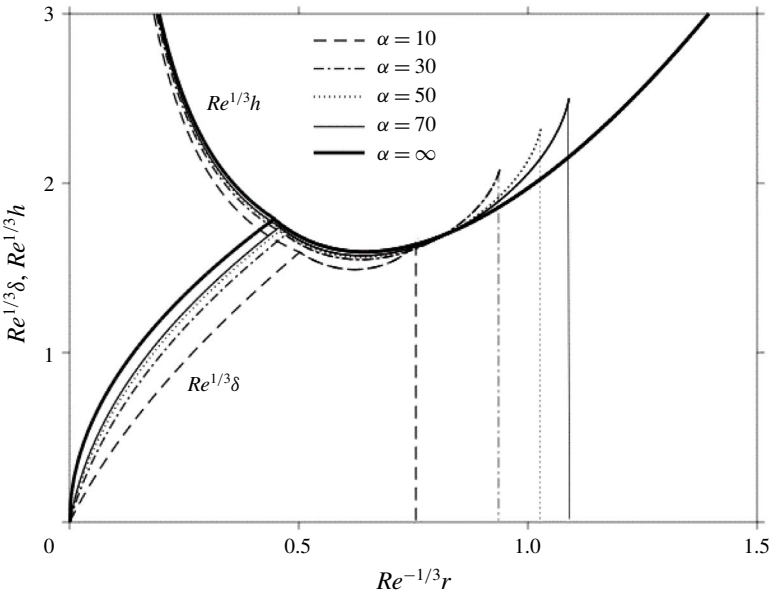

FIGURE 4. Influence of gravity on the developing boundary-layer height and film thickness for supercritical flow. Also indicated in vertical lines are the locations of the hydraulic jump location $Re^{-1/3}r_J$ for different α values.

decreases monotonically with distance downstream of the transition location. In the absence of gravity ($\alpha \to \infty$), the surface velocity decreases rapidly. This behaviour is easily deduced from (4.2) by substituting (4.6) to obtain

$$\bar{U}(\bar{r}_0 < \bar{r} < \bar{r}_J) \sim \tfrac{4}{5}\left(\tfrac{175}{136}(\bar{r}^3 - \bar{r}_0^3) + 2\bar{r}_0\sqrt{\tfrac{70}{39}\bar{r}_0}\right)^{-1}, \quad \text{as } \alpha \to \infty. \tag{4.11}$$

In this case, U decreases like r^{-3} at large distance. The figure indicates that gravity tends to enhance the radial flow near the transition point similar to the effects of disk rotation (Wang & Khayat 2018) and slip (Prince *et al.* 2012; Khayat 2016). The rate at which the surface velocity decays with radial distance is also enhanced by gravity. However, further downstream, gravity inhibits flow movement as the film thickens ahead of the jump.

Figure 6 illustrates the development of the dimensionless wall shear stress at the disk (skin friction) for the same gravity levels as in figures 4 and 5. The figure shows that the wall shear stress is always larger for higher gravity except near the jump. This larger shear stress, which reflects a larger shear rate at the disk, is the result of a thinner film thickness and a greater free-surface velocity caused by a higher gravity effect as already reported in figures 4 and 5. The shear stress decays rapidly with radial distance in the developing boundary-layer region. In the absence of gravity,

$$\bar{\tau}_w(\bar{r}_0 < \bar{r} < \bar{r}_J) \sim \tfrac{6}{5}\bar{r}\left[\tfrac{175}{136}(\bar{r}^3 - \bar{r}_0^3) + 2\bar{r}_0\sqrt{\tfrac{70}{39}\bar{r}_0}\right]^{-2}, \quad \text{as } \alpha \to \infty. \tag{4.12}$$

For any gravity level, after the rapid drop, τ_w exhibits a maximum before decaying monotonically. At large radial distance, the shear stress decays like r^{-5} in the absence

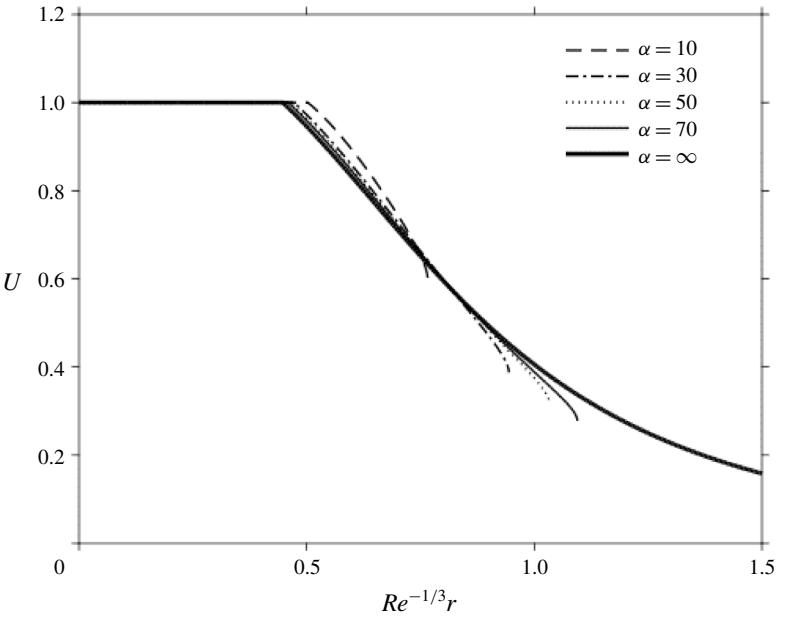

FIGURE 5. Influence of gravity on the free-surface velocity for supercritical flow.

of gravity effect. The strength of the maximum is essentially uninfluenced by gravity, but tends to occur further downstream with increasing gravity effect.

Although both the film height in figure 4 and the free-surface velocity in figure 5 are not significantly influenced by gravity, the location of the jump reflects a significant influence. This is depicted in figure 7 where the jump radius and corresponding film thickness immediately upstream of the jump are plotted against α. The growth of the jump radius and the height closely follows the overall behaviour $\bar{r}_J \approx \alpha^{1/6}$ and $\bar{h}_J \approx \alpha^{2/9}$, yielding $\bar{r}_J^2 \bar{h}_J^3 \approx \alpha$, which agrees with the original expression (4.10). The fractional power growth is also reflected from the position of the vertical lines in figure 4 as well.

4.3. *Comparison with experiment*

Figure 8 shows the dependence of the dimensional jump location on the flow rate, where comparison is carried out with the measurements of Hansen *et al.* (1997) as well as the numerical predictions of Rojas *et al.* (2010) for silicon oils of two different viscosities. The same experimental data were also used by Rojas *et al.* (2010) when they validated their spectral solution. We have included our results using the same log–log ranges used by Rojas *et al.* (2010) in their figure 2. Our predictions are in excellent agreement with their numerical results. The qualitative and quantitative agreement for the highest-viscosity case $\nu = 95$ cS is especially encouraging given the simplicity of the present approach compared to their spectral approach. In particular, and in contrast to the numerical approach, the present formulation does not require imposing a boundary condition downstream of the jump. The agreement with experiment appears to suggest that the location of the jump can be determined without knowledge of downstream conditions such as the disk diameter or the thickness at the edge of the disk. This observation corroborates

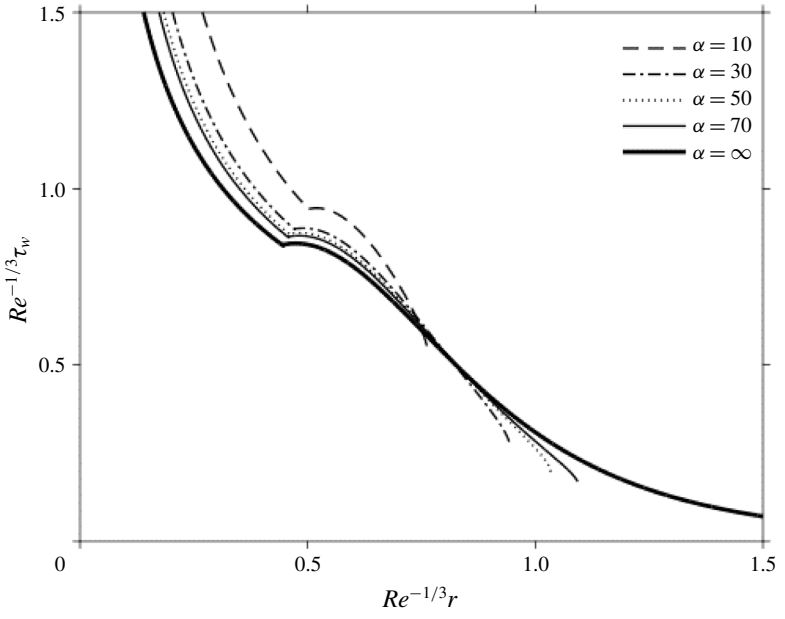

FIGURE 6. Influence of gravity on the wall shear stress for supercritical flow.

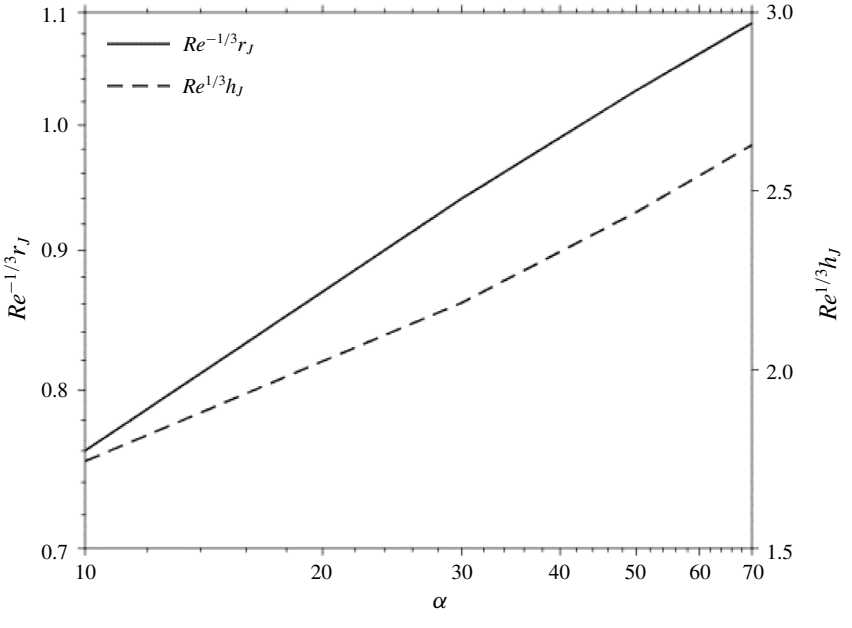

FIGURE 7. Dependence on the jump location and height immediately upstream of the jump on α.

well the experimental findings of Brechet & Neda (1999). We recall that Rojas *et al.* (2010) had to impose the thickness at the edge of the disk as measured by Hansen *et al.* (1997). Both the present theoretical and existing numerical predictions tend

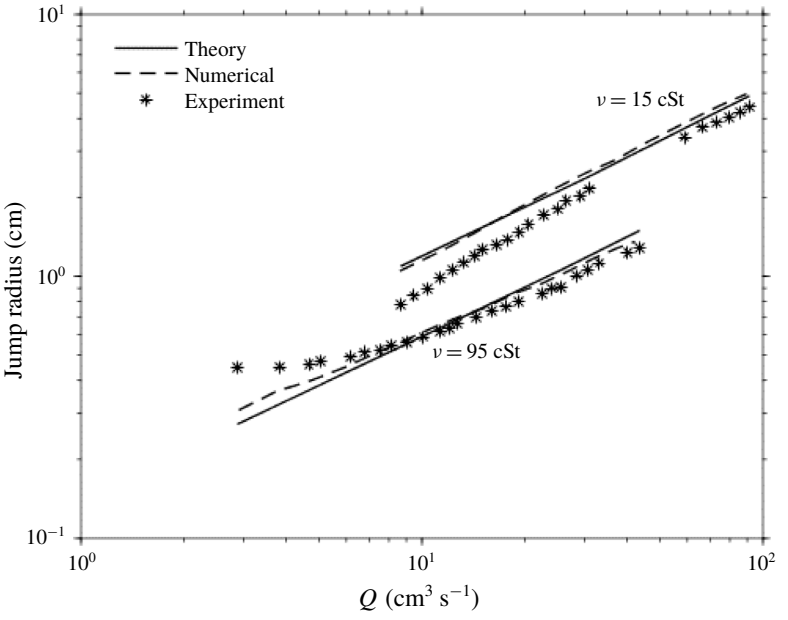

FIGURE 8. Dependence of the hydraulic jump radius on the flow rate. The figure shows the comparison between the present theoretical predictions and the measurements of Hansen *et al.* (1997) for two silicon oils of viscosities $\nu = 15$ cSt and 95 cSt. The numerical predictions of Rojas *et al.* (2010) are also included.

to overestimate slightly the jump radius compared to experiment. The discrepancy appears to be higher for low flow rates, for a given liquid. A plausible explanation for the discrepancy is the difficulty to accurately locate the jump radius in reality. Moreover, it is likely that the jump for $\nu = 95$ cSt is of type II, with two vortex rolls downstream of the jump.

We further assess the validity of our approach by comparison against the scaling law proposed by Rojas *et al.* (2013), which relates the radius of the jump, in particular, to the height downstream of the jump (see their relation (15)). In the absence of surface tension, the relation, written here as $R_J \approx ((9/70)(Q^3/\pi^3 \nu g \tilde{H}_\infty))^{1/4}$, becomes based on their spectral approach for inertial lubrication flow (Rojas *et al.* 2010) and the inviscid Belanger equation (White 2006). Figure 9 shows the comparison between our predictions and the scaling law.

Finally, we observe that our earlier approach (Wang & Khayat 2018), where gravity is neglected in the supercritical regime, could not capture the location of the jump in comparison to experiment for heavily viscous liquids. On the other hand, the case of water is not considered here, not just because of the low viscosity but also due to the high surface tension. We considered the case of water in our recent work dealing with high surface tension liquids along with comparisons with experiment (Wang & Khayat 2018). In the present work, we neglect surface tension upstream in order to investigate the role of gravity on the hydraulic jump. Our objective is to also confirm or dismiss the claim and observation of Duchesne *et al.* (2014) for highly viscous liquids. Further comparison with other existing measurements, including those of Duchesne *et al.* (2014), will be carried out in § 5.

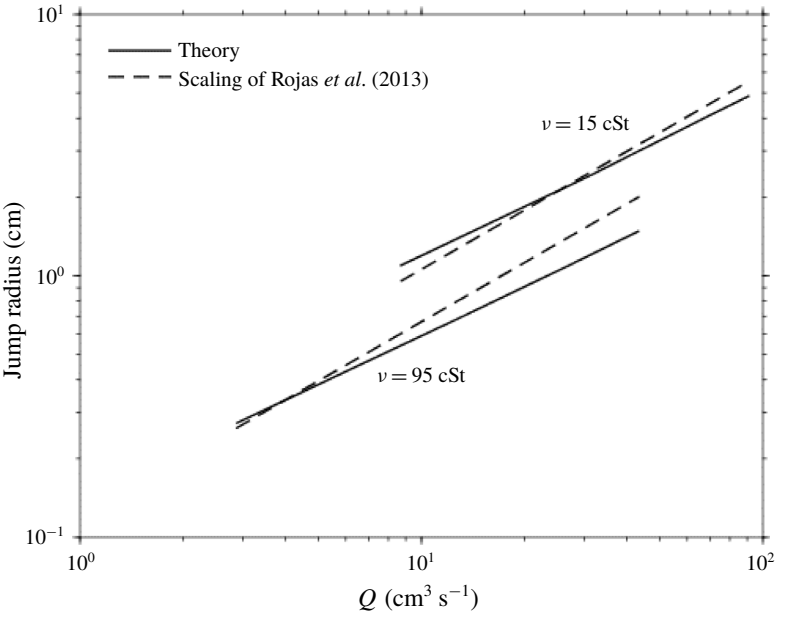

FIGURE 9. Dependence of the hydraulic jump radius on the flow rate. The figure shows the comparison between the present theoretical predictions (solid lines) and the ones based on the scaling law (dashed lines) of Rojas *et al.* (2013) for two silicon oils of viscosities $\nu = 15$ cSt and 95 cSt.

4.4. *Further validation*

As further general assessment of the validity of equation (4.9), we examine its solution against that of the shallow-water equations for weak gravity. Thus, we set $\varepsilon \equiv \alpha^{-1}$ as the small parameter, and expand the thickness as $\bar{h}(\bar{r}) = \sum_{m=0} \varepsilon^m \bar{h}_m(\bar{r})$. To leading order, (4.9) yields the following equation for $\bar{h}_0$:

$$(\bar{r}\bar{h}_0)' = \tfrac{525}{136}\bar{r}^2, \tag{4.13}$$

which corresponds to the thickness in the absence of gravity. The solution of this equation was already given earlier and is equivalent to (4.6). To next order:

$$(\bar{r}\bar{h}_1)' = \tfrac{875}{272}\bar{r}^3\bar{h}_0^3\bar{h}_0'. \tag{4.14}$$

We next examine the corresponding solution of the shallow-water equations, which are first rescaled to involve the only parameter $\alpha = Re^{1/3}Fr^2$ by recalling (3.7) and introducing all the barred variables as

$$r = Re^{1/3}\bar{r}, \quad h = Re^{-1/3}\bar{h}, \quad z = Re^{-1/3}\bar{z}, \quad u = \bar{u}, \quad w = Re^{-2/3}\bar{w}. \tag{4.15a–e}$$

In this case, equations (2.1*a*), (2.5) and (2.6) become

$$\bar{u}_{\bar{r}} + \frac{\bar{u}}{\bar{r}} + \bar{w}_{\bar{z}} = 0, \quad \bar{u}\bar{u}_{\bar{r}} + \bar{w}\bar{u}_{\bar{z}} = -\alpha^{-1}\bar{h}' + \bar{u}_{\bar{z}\bar{z}}, \quad \int_0^{\bar{h}} \bar{u}\,\mathrm{d}\bar{z} = \frac{1}{2\bar{r}}. \tag{4.16a–c}$$

In the presence of gravity, a similarity solution is possible only under some conditions.

Starting with the mapping $\bar{\xi}(\bar{r},\bar{z})=\bar{r}$, $\bar{\eta}(\bar{r},\bar{z})=\bar{z}/\bar{h}(\bar{r})$, and taking $\bar{u}(\bar{r},\bar{z})=\bar{U}(\bar{\xi})g(\bar{\eta})$, (4.16*a*) becomes

$$\bar{U}'g-\frac{\bar{h}'}{\bar{h}}\bar{\eta}\bar{U}g_{\bar{\eta}}+\frac{\bar{U}g}{\bar{\xi}}+\frac{1}{\bar{h}}\bar{w}_{\bar{\eta}}=0. \tag{4.17}$$

Isolating $\bar{w}_{\bar{\eta}}$ and rearranging terms:

$$\bar{w}_{\bar{\eta}}=\bar{\xi}^{-1}[-(\bar{\xi}\bar{h}\bar{U})'g+\bar{\xi}\bar{h}'\bar{U}(\bar{\eta}g)_{\bar{\eta}}]. \tag{4.18}$$

Now, from conservation of mass or (4.16*c*), we have

$$\bar{U}\bar{h}\bar{r}=\frac{1}{2\displaystyle\int_0^1 g\,\mathrm{d}\bar{\eta}}=\text{Const., yielding}\quad(\bar{\xi}\bar{h}\bar{U})'=0. \tag{4.19}$$

Consequently, (4.18) reduces to $\bar{w}_{\bar{\eta}}=\bar{h}'\bar{U}(\bar{\eta}g)_{\bar{\eta}}$. Integrating and recalling that $\bar{w}(\bar{\xi},\bar{\eta}=0)=0$, we get $\bar{w}=\bar{h}'\bar{U}\bar{\eta}g(\bar{\eta})$.

We thus have so far

$$\bar{u}=\bar{U}g(\bar{\eta}),\quad \bar{w}=\bar{h}'\bar{U}\bar{\eta}g(\bar{\eta}),\quad \bar{r}\bar{U}\bar{h}=C\equiv\left(2\int_0^1 g(\eta)\,\mathrm{d}\eta\right)^{-1}, \tag{4.20a–c}$$

where (4.20*c*) is deduced from (4.16*c*). Substituting the velocity components from (4.20*a*,*b*) into equation (4.16*b*), and eliminating $\bar{U}$ using (4.20*c*), yields the following problem for g:

$$C^2(\bar{r}\bar{h})'g^2-\varepsilon\bar{h}^3\bar{r}^3\bar{h}'+Cr^2g_{\bar{\eta}\bar{\eta}}=0,\quad g(0)=g_{\bar{\eta}}(1)=0,\quad g(1)=1. \tag{4.21a–c}$$

We again seek the solution by expanding the thickness as $\bar{h}(\bar{r})=\sum_{m=0}\varepsilon^m\bar{h}_m(\bar{r})$. To leading order, we recover the classical equation of Watson (1964):

$$C(\bar{r}\bar{h}_0)'g^2+\bar{r}^2g_{\bar{\eta}\bar{\eta}}=0, \tag{4.22}$$

which suggests that $\bar{r}^{-2}(\bar{r}\bar{h}_0)'$ must be constant. Multiplying (4.22) by $g_{\bar{\eta}}$, and integrating using the conditions in (4.21), yields the following equation:

$$(rh_0)'=\frac{3c^2}{2C}r^2,\quad \text{where } c=\int_0^1\frac{\mathrm{d}g}{\sqrt{1-g^3}}=1.402. \tag{4.23}$$

The value of C is determined by noting that $c=g_{\bar{\eta}}/\sqrt{1-g^3}$, yielding $\int_0^1 g\,\mathrm{d}g=\int_0^1 g\,\mathrm{d}g/\sqrt{1-g^3}=0.615$, so that $C=0.813$. To the next order in ε, (4.21) gives

$$(\bar{r}\bar{h}_1)'=\frac{3c}{2C^2}\bar{r}^3\bar{h}_0^3\bar{h}_0', \tag{4.24}$$

where $c\int_0^1 g^2\,\mathrm{d}\eta=(1/3)\int_0^1\mathrm{d}g^3/\sqrt{1-g^3}=2/3$ was used. Comparison between the numerical coefficients of (4.14) and (4.24) indicates a discrepancy of 6 %. The discrepancy for the first-order contribution is 1 % when (4.15) is compared with (4.24).

Finally, it is worth observing that Bohr *et al.* (1993) and Rojas *et al.* (2013) found that the jump radius scales roughly as $R_J \approx Q^{5/8}\nu^{-3/8}g^{-1/8}$. Using the current scaling, the dimensionless form of the estimate of Bohr *et al.* can be written as $r_J \approx Re^{3/8}Fr^{1/4}$. Avedisian & Zhao (2000) investigated the circular hydraulic jump experimentally for normal and reduced gravity conditions. They measured the jump diameter and shape at the free liquid surface for an impinging jet on a stationary disk. Based on the reported two values of the flow rate and two gravitational acceleration data provided, we find that the location of the jump behaves close to $g^{-1/9}$, roughly confirming the scaling of Bohr *et al.* (1993) for low gravity. We can also estimate the behaviour of the jump radius from (4.8) by assuming the thickness from (4.6) or (4.7) for large distance or $h_J \approx r_J^2/Re$. When inserted in (4.8), we obtain $r_J \approx Re^{3/8}Fr^{1/4}$, which is precisely the scaling suggested by Bohr *et al.* (1993) cast in dimensionless form. Interestingly, this scaling law can also be expressed in terms of only one parameter as $\bar{r}_J \approx \alpha^{1/8}$.

5. The influence of gravity on the hydraulic jump height and the subcritical flow

Now that the jump location has been determined, we are in a position to examine the flow and the film height in the subcritical region downstream of the jump, in particular the height of the jump. Here, we consider two alternatives and assess their validity, the first consisting of applying the conservation of momentum across the jump, and the second involving the use of the film thickness at the edge of the disk and integrating the momentum equation (backwards) to determine the jump height. We conveniently let $r = r_{J-}$ and $r = r_{J+}$ denote the radial position immediately up- and downstream of the jump, respectively, with corresponding film heights $h_J \equiv h(r = r_{J-})$ and $H_J \equiv h(r = r_{J+})$.

5.1. *Conservation of momentum across the jump*

We first recall the integral form (4.3) of the momentum conservation equation, which holds for any position $r > r_0$ in the super- and subcritical regions. Across the jump, equation (4.3) is applied for a control volume of width Δr in the radial direction, taking the following discretized form:

$$Re\Delta \int_0^h u^2 \,\mathrm{d}z = -\frac{Re}{Fr^2}\frac{\Delta h^2}{2} - \Delta r u_z(r_J, z=0). \tag{5.1}$$

Since the width of the jump Δr is assumed to be small, equation (5.1) reduces to

$$\frac{Fr^{-2}}{2}(H_J^2 - h_J^2) = \int_0^{h_J} u^2(r_{J-}, z)\,\mathrm{d}z - \int_0^{H_J} u^2(r_{J+}, z)\,\mathrm{d}z. \tag{5.2}$$

We observe that the supercritical velocity is already available from (4.1) and (4.2), yielding $u(r_{J-}, z) = (4/5r_J h_J)f(\eta)$, where $\eta = z/h_J$ and $f(\eta)$ is given in (3.4). We also use relation (4.8) to eliminate h_J, In this case, (5.2) becomes

$$H_J^2 - 3\left(\frac{272}{875}\frac{Fr^2}{r_J^2}\right)^{2/3} + 2Fr^2\int_0^{H_J} u^2(r_{J+}, z)\,\mathrm{d}z = 0. \tag{5.3}$$

Thus, the jump height is completely determined as a function of the Froude and the Reynolds numbers once the subcritical velocity profile $u(r_{J+}, z)$ is imposed.

Various assumptions have been adopted in the literature, ranging from inviscid to fully viscous flows. Both regimes will be explored next.

We first consider the flow to be inviscid downstream of the jump. Although the present work is focused on heavily viscous liquids, the inviscid subcritical flow would correspond to a jump that is relatively high. A boundary layer always exists, but it is relatively thin in this case. Consequently, the velocity right downstream of the jump would be essentially uniform. This is an assumption that has been widely adopted in the literature in various contexts (see, for instance, Watson 1964; Bush & Aristoff 2003; Dressaire *et al.* 2010; Prince *et al.* 2012). At the very least, the inclusion of the uniform subcritical flow is helpful as a reference limit. The assumption of uniform flow does not necessarily have to hold over the entire domain downstream of the jump. It is not unreasonable to assume that the velocity is uniform right downstream of the jump, which allows the jump height to be readily determined from (5.3). Further downstream, the flow may be considered fully viscous, and can be determined by taking the jump height and velocity as initial conditions.

Thus, assuming uniform flow downstream of the jump, and using the mass conservation equation (2.6), equation (5.3) reduces to

$$H_J^2 - 3\left(\frac{272}{875}\frac{Fr^2}{r_J^2}\right)^{2/3} + \frac{Fr^2}{2r_J^2 H_J} = 0. \tag{5.4}$$

Equation (5.4) takes an interesting form when cast in terms of the Froude number based on the jump radius and height. In this regard, there is a close connection with the recent experimental findings and claim of Duchesne *et al.* (2014), which we will now explore.

Duchesne *et al.* (2014) introduced the Froude number defined in terms of the jump height and the average velocity immediately after the jump, namely $Fr_J = Fr/2r_J H_J^{3/2}$ in our notations. Their measurements suggest that Fr_J remains sensibly independent of the flow rate (constant with respect to Fr). However, they could not explain or theoretically support this observation, which, in turn, begs the question whether the constancy of Fr_J has any theoretical basis. This turns out to be indeed the case as we shall now demonstrate.

It is easy to see that (5.4) yields the following equation for Fr_J:

$$Fr_J^2 - \tfrac{24}{25}(\tfrac{17}{7})^{2/3} Fr_J^{4/3} + \tfrac{1}{2} = 0. \tag{5.5}$$

This equation indicates that Fr_J is indeed a constant that is independent of the Fr or, equivalently, of the flow rate, confirming the observation of Duchesne *et al.* (2014). This is a cubic equation in $Fr_J^{2/3}$, admitting $Fr_J = 0.58$ as a solution. Thus, we have established the constancy of Fr_J when the subcritical flow to be inviscid.

We next address the question whether Fr_J remains actually independent of the flow rate if the subcritical flow is assumed to be viscous, and see whether this yields a closer constant Fr_J value to the one measured by Duchesne *et al.* (2014). We follow Duchesne *et al.* (2014), and adopt a lubrication flow approach. In this case, a differential equation for H can be obtained by neglecting the inertial terms in equation (2.5), yielding the following profile for the radial velocity:

$$u(r > r_J, z) = \frac{Re}{Fr^2}\frac{\mathrm{d}H}{\mathrm{d}r}\left(\frac{z^2}{2} - Hz\right). \tag{5.6}$$

Inserting u into the mass conservation (2.6) and integrating, the equation governing the film thickness downstream of the jump becomes

$$\frac{\mathrm{d}H}{\mathrm{d}r} = -\frac{3}{2}\frac{Fr^2}{Re}\frac{H^{-3}}{r}, \tag{5.7}$$

which leads to the velocity profile just downstream of the jump as

$$u(r_{J+}, z) = -\frac{3}{2r_J H_J^3}\left(\frac{z^2}{2} - H_J z\right). \tag{5.8}$$

Finally, inserting (5.8) into (5.3), we obtain the following equation for Fr_J:

$$Fr_J^2 - \tfrac{4}{5}(\tfrac{17}{7})^{2/3} Fr_J^{4/3} + \tfrac{5}{12} = 0. \tag{5.9}$$

Similar to (5.5), equation (5.9) also confirms that Fr_J is independent of Fr (flow rate), with $Fr_J = 0.71$.

What we have established so far, based on the discretized mass and momentum equations across the jump, is that Fr_J is indeed constant (independent of the flow rate) as Duchesne *et al.* (2014) claim from their measurements. Surprisingly, this is the case whether the subcritical flow is assumed to be inviscid or viscous obeying the lubrication regime, thus covering a wide range of viscosity and flow rate. The value of Fr_J is found to be slightly lower for inviscid compared to viscous subcritical flow. However, both values remain higher than the measured value by Duchesne *et al.* (2014): $Fr_J \approx 0.35$–0.40. It is important to observe that the values of Fr_J can be found theoretically without the knowledge of downstream conditions of the jump such as the disk radius or the thickness at the edge of the disk. Such conditions are not needed when the discretized conservation equations are invoked. Another important observation to make is whether the discretized (5.2) itself is valid. It is expected that (5.2) remains reasonably valid for low-viscosity liquids or at high flow rate since the jump is of negligible thickness and its location is well defined. However, for high-viscosity liquids such as the silicon oils used by Duchesne *et al.* (2014), the jump is expected to be wide, and (5.2) cannot be entirely valid. This brings us to the second alternative when seeking the subcritical flow.

5.2. *The influence of disk radius and edge thickness*

We proceed by examining the flow in the subcritical range, downstream of the jump, without invoking (5.3). In this case, an approximate or asymptotic solution of (4.4) can be found by keeping the three dominant terms for large distance, reducing it to a lubrication-like equation for H:

$$\frac{\mathrm{d}H}{\mathrm{d}r} = -\frac{6}{5}\frac{Fr^2}{Re}\frac{H^{-3}}{r}. \tag{5.10}$$

Subject to $H(r = r_\infty) = H_\infty$, (5.10) can be integrated analytically to give

$$H(r) = \left(H_\infty^4 + \frac{24}{5}\frac{Fr^2}{Re}\ln\left(\frac{r_\infty}{r}\right)\right)^{1/4}. \tag{5.11}$$

The prediction of the edge thickness was considered in our recent study for the flow on a rotating disk (Wang & Khayat 2018). The case of a stationary disk was

also examined. Both static and dynamic contributions were considered, which yielded an accurate prediction established by comparing against experiment for the edge thickness. Direct measurements by Duchesne *et al.* (2014) of the edge thickness, performed at nearly 5 mm of the disk perimeter in their experiment, give a nearly constant value of 1.5 mm with a weak power-law variation with the flow rate, not exceeding a few per cent. This constant thickness value, for a liquid of surface tension γ, is very close to the capillary length $\sqrt{\gamma/\rho g}$ of the fluid, which results from the balance of forces between the hydrostatic pressure and the surface tension at the disk perimeter. This value is also consistent with the measurements of Dressaire *et al.* (2010). Consequently, we assumed that the film thickness at the edge of the disk is essentially equal to the film thickness the liquid exhibits under static conditions. Lubarda & Talke (2011) proposed an expression for this static thickness as $h_s = 2\sqrt{\gamma/\rho g}\sin(\theta_Y/2)$, based on the minimum free energy principle. Here θ_Y is the contact angle, which depends on both the liquid and the solid, and may then be deduced from experiment. For water, we achieved an excellent agreement with the measurements of Dressaire *et al.* (2010) for the jump radius by taking $\theta_Y = 90°$. This value is within the range of values measured for water on polydimethylsiloxane (Diversified Enterprises 2009), which is the material used by Dressaire *et al.* (2010) for their disk. For water flowing on glass, $\theta_Y = 35°$ (Vicente, Andre & Ferreira 2012), a value used recently in our comparison with the measurements of Hansen *et al.* (1997) for water (Wang & Khayat 2018).

In addition to the static contribution, and in order to explore the small variation of edge thickness with flow rate as observed by Duchesne *et al.* (2014), we resorted to a minimum mechanical energy principle (Yang & Chen 1992; Yang, Chen & Hsu 1997), which states that a fluid flowing over the edge of a disk under the influence of a hydrostatic pressure gradient will adjust itself so that the mechanical energy within the fluid will be minimum with respect to the film thickness at the disk edge. Consequently, the contribution to the thickness at the edge of the disk is determined by setting the derivative of the mechanical energy with respect to the film thickness equal to zero. In dimensionless form, the total energy is $E = \int_0^H (Fr^2(u^2/2) + z + p)\,\mathrm{d}z$. Since the pressure is hydrostatic: $p = -z + H$, yielding $E = \int_0^H (Fr^2(u^2/2) + H)\,\mathrm{d}z$. Consequently, we set $\partial/\partial H \int_0^H (Fr^2(u^2/2) + H)\,\mathrm{d}z = 0$ at the edge of the disk. Using (5.8), we obtain the dimensionless film thickness at the edge as

$$H_\infty = 2\sqrt{\frac{1}{Bo}}\sin\left(\frac{\theta_Y}{2}\right) + \left(\frac{3}{40}\right)^{1/3}\left(\frac{Fr}{r_\infty}\right)^{2/3}. \tag{5.12}$$

Here the Bond number is given by $Bo = \rho g a^2/\gamma$. Clearly, in the presence of relatively strong gravity or surface tension and large disk radius, the second term tends to be dominated by the static contribution. As we shall see next, even the static contribution will turn out to be uninfluential for the heavily viscous liquids considered in the present work.

Indeed, once the thickness $H(r = r_\infty) = H_\infty$ at the edge of the disk is determined as per (5.12), we obtain the film thickness distribution downstream of the jump from (5.10). In particular, and given that the jump location has already been determined, the jump height is now obtained through

$$H_J = \left(H_\infty^4 + \frac{24}{5}\frac{Fr^2}{Re}\ln\left(\frac{r_\infty}{r_J}\right)\right)^{1/4}. \tag{5.13}$$

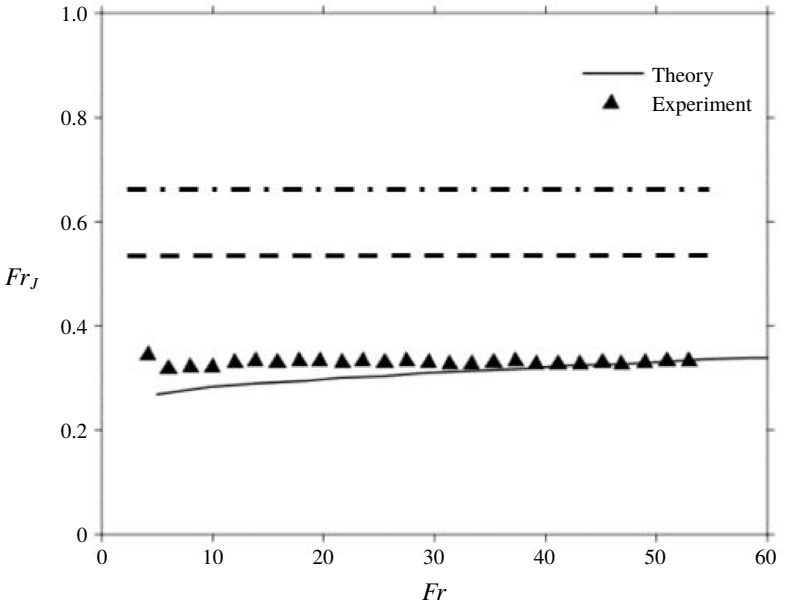

FIGURE 10. Dependence of Fr_J on the flow rate (Froude number). The solid line correspond to predictions based on relations (4.4) and (5.13). The experimental data corresponding to silicon oil are from Duchesne *et al.* (2014). Also added as dashed and dash-dotted lines the result based on (5.5) and (5.9), respectively.

In this case, it is not difficult to confirm that, for a large disk and relatively small Reynolds number, the logarithmic term dominates on the right-hand side of (5.13). This is obviously the case of very viscous liquids. As a comparison, the Reynolds number for the flow of silicon oils (Duchesne *et al.* 2014) is of the order of 10^2, whereas for water (Dressaire *et al.* 2010) its order is closer to 10^4. It is important to note that the range of Froude number in both sets of measurements is essentially the same. Based on the range of Froude numbers in figure 10 below, it is not difficult to deduce that the static contribution to the edge thickness is also dominated. In fact, experiment (Duchesne *et al.* 2014) indicate that $H_\infty = O(1)$ at most, and $H_\infty \approx 0$ for a liquid of high viscosity.

We now turn, once again, to examining conditions where Fr_J may remain independent of the flow rate. This time, (5.13) is used instead of (5.3). In this case, since the pre-jump height h_J and the jump radius r_J must be computed numerically, it is not possible to derive a closed form equation similar to (5.5) or (5.9), confirming that Fr_J is constant. In fact, (5.13) suggests that Fr_J is not independent of Fr. However, the dependence on Fr turns out to be weak, as figure 10 suggests. The figure shows the variation of Fr_J against Fr for the silicon oil of viscosity 20 cSt used by Duchesne *et al.* (2014) in their measurements, which are also shown in the figure. The experimental data are reproduced in dimensionless form. Surprisingly, the figure indicates that Fr_J not only is indeed sensibly constant but agrees closely with experiment. Some discrepancy is, however, noted for low flow rates, which is not surprising given the difficulty in measuring accurately the jump radius and height.

Now that the solution is available in the supercritical and subcritical regions, we are in a position to validate our model over the entire domain, against existing numerical results and experiment. We also take the opportunity to assess the validity of the parabolic profile. For the supercritical range, an equation similar to (4.4) is obtained when using the parabolic profile: $f(\eta) = 2\eta - \eta^2$, namely

$$Re\left(\frac{1}{Fr^2} - \frac{3}{10r^2h^3}\right)h' = \frac{3}{10rh^2}\left(\frac{Re}{r^2} - \frac{5}{h}\right). \tag{5.14}$$

We observe that the asymptotic form of (5.14) for large r is precisely the lubrication (5.7), which when integrated yields

$$H(r) = \left(H_\infty^4 + 6\frac{Fr^2}{Re}\ln\left(\frac{r_\infty}{r}\right)\right)^{1/4}. \tag{5.15}$$

Figure 11 shows the comparison between the present theory and the numerical results of Rojas & Tirapegui (2015) as well as the measurements of Ellegaard *et al.* (1996) for ethylene glycol. Both formulations based on the parabolic and cubic profiles are represented. The results for the free-surface velocity are reported in dimensionless form, with corresponding parameters being $Re = 334$, $Fr = 14.4$ and $Bo = 1.21$. The contact angle used to determine the edge thickness is $\theta_Y = 70°$, yielding a total edge thickness of $H_\infty = 1.7$, including the height of the vertical edge. While the position of the jump is well reproduced by the present theory based on the cubic profile and the numerical method, figure 11 shows that the theory tends to slightly underestimate the level of the surface velocity in both the super- and subcritical ranges. Figure 11 indicates that the numerical approach of Rojas *et al.* tends to agree slightly better with experiment than the present theory. The figure also indicates a larger discrepancy when the parabolic profile is used.

We next examine the shape of the entire film under general flow conditions. For this, we rescale (5.11) using (3.7) to reduce the problem in terms of the parameter α:

$$\bar{H}(\bar{r}) = \left(\bar{H}_\infty^4 + \frac{24}{5}\alpha\ln\left(\frac{\bar{r}_\infty}{\bar{r}}\right)\right)^{1/4}. \tag{5.16}$$

Here $\bar{H}_\infty = 2\sqrt{Re^{2/3}/Bo}\sin(\theta_Y/2) + ((3/40)\alpha/\bar{r}_\infty^2)^{1/3}$ from (5.12). The overall effect of gravity is illustrated in figure 12, which depicts the film thickness over the entire disk. The jump height decreases with increasing gravity, simultaneously as the jump location is pushed upstream toward the stagnation point and away from the edge of the disk. We can also observe the logarithmic increase in height reported earlier in figure 7.

While the use of (4.4) or (4.9) is imperative in the supercritical range ahead of the jump, allowing us to locate the jump, it is not necessarily so for the subcritical flow, where we have the choice to use different approximations. For instance, as the flow slows down downstream of the shock, we saw that the lubrication assumption holds well between the jump and the edge of the disk, yielding a good agreement with experiment (see figures 10 and 11). Our calculations of the subcritical flow so far are based on the asymptotic form (5.11) of (4.4) or (5.16) of (4.9) for large r as it is convenient to use, given the analytical distribution of the thickness (and velocity) downstream of the jump and its direct relation to the edge thickness and

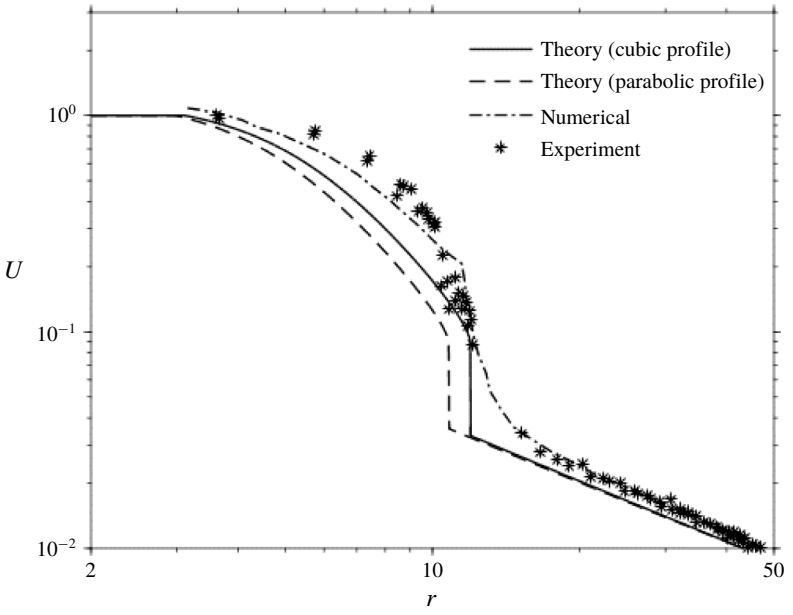

FIGURE 11. Free-surface velocity in the supercritical and subcritical domains. Comparison between the present theory (solid line), the numerical results of Rojas & Tirapegui (2015), as well as the experimental data of Ellegaard *et al.* (1996). Also added is the velocity distribution based on the parabolic profile.

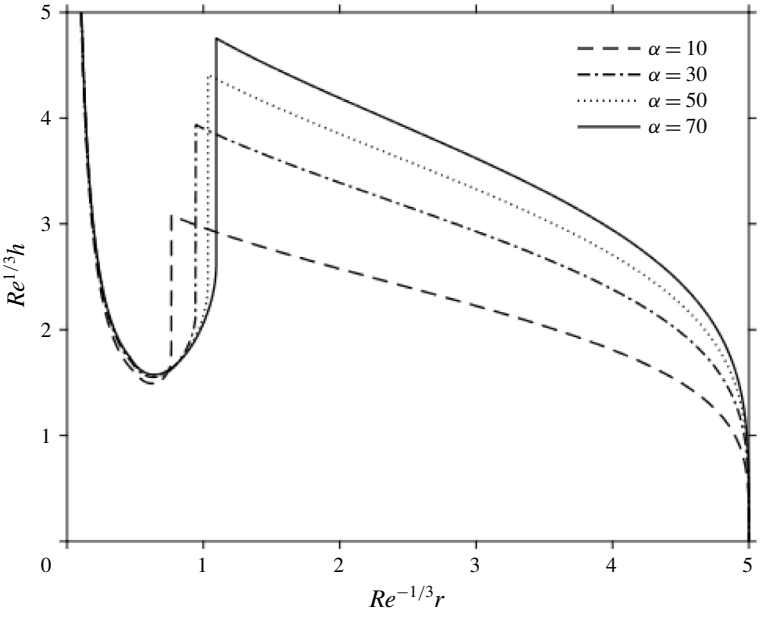

FIGURE 12. Influence of gravity on the film thickness plotted against radial distance in regions (ii), (iii) and (iv).

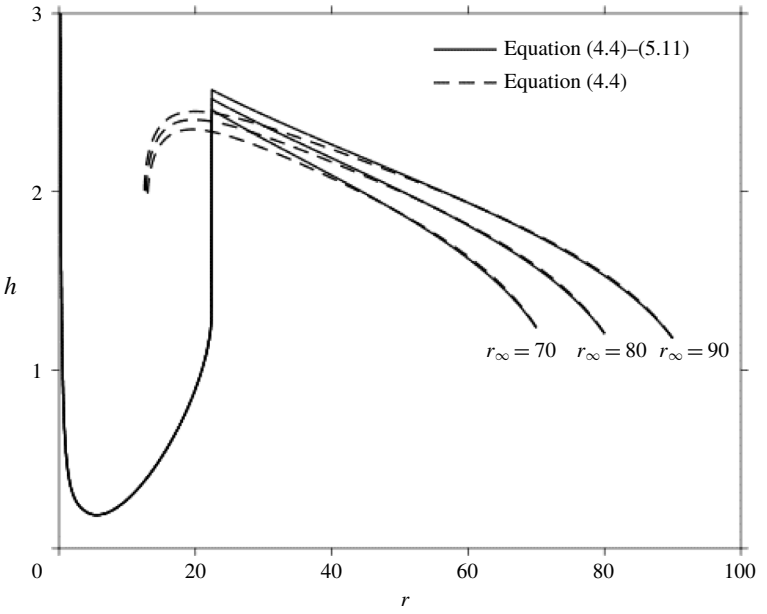

FIGURE 13. Influence of the disk radius on the film thickness plotted against the radial distance in regions (ii), (iii) and (iv). Solution in solid line based on equations (4.4) and (5.11). Dashed line shows the subcritical profile based on (4.4).

the disk radius. Alternatively, we now consider using (4.4), and apply it directly to capture the subcritical flow, which should allow us to assess the validity of (5.11). Simultaneously, we examine the effect of the disk radius. The comparison is reported in figure 13 for the film thickness distribution with distance in the super- and subcritical ranges for three different values of the disk radius. We take $Re = 628$, $Fr = 63$, $Bo = 1.1$ and $\Theta_Y = 55°$. In this case, the values of the thickness at the edge of the disk are determined from (5.12) are $H_\infty = 1.24$, 1.2 and 1.18, corresponding to $r_\infty = 70$, 80 and 90, respectively.

Several observations are worth making here. Figure 13 shows that the subcritical branches exhibit a turning point corresponding to the singularity of (4.4), which occurs slightly upstream of the jump location. As expected, the profile of the asymptotic solution (5.11) collapses onto the profile based on (4.4) at a distance not too far from the jump. This distance, nevertheless, increases with the disk radius. The asymptotic solution yields a jump height H_J that is slightly above the one based on the exact solution of (4.4). Finally, despite the important spread in the values of the disk radius, the location of the singularity reached by the subcritical branches is essentially the same, as reflected in the saturation near the turning point. This seems to suggest that the location of the jump in reality, if it were to fall half-way, say, between the two locations of the singularity, is independent of downstream conditions. We seem to reach this observation regardless of which branch, super- or subcritical, we are referring to.

Next, we pursue our assessment of the validity of (4.4) and the asymptotic form (5.11) against experiment. The comparison is reported in figure 14 for the film thickness distribution with distance in the super- and subcritical regions against the measurements of Duchesne *et al.* (2014) for silicon oil (20 cSt). The data are

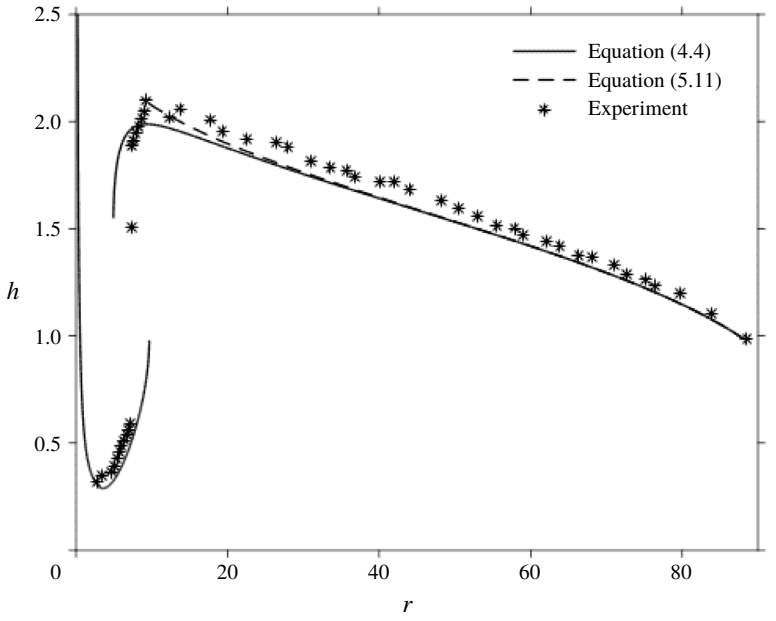

FIGURE 14. Free-surface profile. Comparison between theoretical predictions and the measurements of Duchesne *et al.* (2014) for silicon oil (20 cSt). Results plotted in dimensionless form with $Re = 169$, $Fr = 14.88$, $Bo = 1.19$, $\Theta_Y = 55°$ and $\bar{r}_\infty = 94$. Theoretical profiles based on current theory or (4.4) (solid lines) and asymptotic subcritical (5.11) (dashed line).

reproduced here in dimensionless form from their figure 2, corresponding to $Re = 169$, $Fr = 14.88$, $Bo = 1.19$, $\Theta_Y = 55°$ and $\bar{r}_\infty = 94$. In this case, the value of the thickness at the edge of the disk is determined from (5.12) as $\bar{H}_\infty = 0.95$. Several observations are worth making here. Figure 14 shows that the theoretical predictions, based on the solution of (4.4), are generally in good agreement with the experiment of Duchesne *et al.* (2014), slightly underestimating their measurements. The location of the jump is predicted to be close to the level of the turning point or the singularity of the supercritical branch upstream of the jump. The subcritical branch also exhibits a turning point corresponding to the singularity of (4.4), occurring slightly downstream of the jump location (see figure 13). The behaviour of the two branches is in close (qualitative) agreement with the theoretical predictions of Kasimov (2008) who incorporated the shape of the bottom (flat disk with a sharp cut off at the edge). The reader is particularly referred to figure 3(*a*) from Kasimov (2008). The asymptotic solution cannot mimic the downward turning trend observed in the experiment, yielding a jump height HJ that is slightly above the one based on the exact solution of (4.4). Interestingly, there is no need here to integrate from a critical point coinciding with at the edge of the disk to obtain the subcritical branch as Kasimov (2008) did. Kasimov estimated the location of the jump to be somewhere between the upstream and downstream singularities, which seems to be case here. However, this may not always be the case. Based on the agreement between theory and experiment in previous figures, we saw that the location of the jump coincides rather with the upstream singularity of the averaged momentum equation.

Finally, an interesting observation can be made regarding the (constant) value of Fr_J and its independence of Fr (or the flow rate). The measurements of the film profile for heavily viscous liquids seem to give a rough estimate of the height H_J immediately downstream of the relative the height h_J upstream of the jump. More precisely, experiment suggests that $H_J \approx 2h_J$ (see, for instance, the measurements of Ellegaard *et al.* (1996), and those in figure 2 of Duchesne *et al.* (2014). By substituting $h_J = H_J/2$ in (4.8) and recalling that $Fr_J = Fr/2r_J H_J^{3/2}$, we deduce that

$$Fr_J = \frac{Fr}{2^{5/2} r_J h_J^{3/2}} = \frac{1}{16}\sqrt{\frac{875}{34}} \simeq 0.32, \tag{5.17}$$

which is very close to 0.33, the value measured by Duchesne *et al.* (2014). Another way of obtaining the same result is to assume that the singularity yielding (4.8) occurs at a height half-way along the jump, where we expect the slope to be largest (infinite). In this case, one would replace h_J in (4.8) by the average height, which, in turn, can be approximated as $(H_J + h_J)/2 \approx H_J/2$ if one assumes that $h_J \ll H_J$ (Watson 1964), and obtain (5.17). The estimated value in (5.17) confirms the important observation in this study that the jump characteristics appear to be dictated only by the supercritical flow and upstream conditions.

6. Concluding remarks and discussion

In this study, the flow of a high-viscosity jet impinging on a stationary disk is examined theoretically. The present study focuses on the role of gravity in the prediction of both the location and height of the circular hydraulic jump, and is restricted to laminar circular steady jump of type I, which exhibits a sharp transition and is marked by unidirectional surface flow with boundary-layer separation beyond the jump (Bohr *et al.* 1996; Bush & Aristoff 2003). See figure 1. Despite the numerous theoretical and numerical studies in the literature, this prediction remains somewhat difficult to achieve through a simple and practical theoretical model. This issue was recently addressed in our work on a jet impinging on a rotating disk, but was limited to low-viscosity liquids (Wang & Khayat 2018). Typical theoretical models in the literature seem to rely on some empirical input to generate boundary conditions, or lack the additional relation needed along with the discretized momentum balance across the jump when an approach similar to Watson's is used. The additional relation is needed in order to determine uniquely the location and height of the jump. In the present study, we show how a closure to the problem can be brought by establishing a simple relation between the jump location and pre-jump height by including the effect of gravity in the developing boundary layer and the supercritical region of the flow domain. In fact, we show that the Froude number based on the pre-jump height and jump radius is constant (see relation (4.8) or (4.10)).

The flow is assumed to remain steady and axisymmetric. A model is developed based on the Kármán–Pohlhausen integral approach to describe the behaviour of the flow in the developing boundary-layer region (ii) and the fully developed viscous region (iii). The integral form of the continuity and momentum equations, governing the flow of a thin film, is treated numerically separately in each region, and the flow is matched at the transition point. Unlike the flow in the absence of gravity, the problem does not admit a similarity solution. However, a self-similar cubic profile is nevertheless assumed for the velocity, which is commonly used and was previously shown to be accurate. Although two dimensionless parameters are involved in the

absence of surface tension, namely the Reynolds number Re and the Froude number Fr defined in terms of the jet radius and the flow rate, we show that the problem can be cast in terms of only one parameter: $\alpha = Re^{1/3}Fr^2$.

We find that gravity tends to enhance inertia, leading to a drop in the boundary-layer height as well as the film thickness in region (ii). Near the stagnation point, the boundary layer departs from the $\sqrt{r/Re}$ behaviour to grow increasingly linearly with distance like $\delta \approx \sqrt{3}(Fr/\sqrt{Re})r$ under the influence of gravity. The transition point, where the outer edge of the boundary layer intersects the film surface, moves towards the perimeter of the disk with increasing gravity while the film thickness at the transition location diminishes (figures 2 and 3).

In the fully viscous region (iii), the shallow-water equations are reduced to a first-order equation for the thickness (4.4) or (4.9). We show that this equation exhibits an essential singularity in the presence of gravity at a distance identified as the jump location. As the flow slows down, inertia weakens and friction increases with radial distance. At some distance gravity and viscous effects become equal, causing the singularity and therefore the jump to occur.

The numerical solution indicates that the film thickness decreases rapidly near impingement and exhibits a minimum that strengthens with gravity (figure 4), accompanied by an increase in the surface velocity that decays at a slower rate with radial distance (figure 5). Interestingly, unlike the film thickness, the surface velocity decays monotonically with distance. In contrast, the shear stress along the wall exhibits a weak maximum that shifts downstream as the effect of gravity increases (figure 6).

We show that, for a flat disk, the jump radius can be determined independently of its height or downstream conditions, in agreement with experimental observations. Based on their measurements, Brechet & Neda (1999) concluded that 'the boundary conditions on a perfectly flat plate do not influence the radius of the hydraulic jump'. These findings are validated against existing experimental data and numerical simulation. Comparison between the predicted and measured jump locations in figure 8 confirm that, for a circular jump, the jump radius is independent of the subcritical flow downstream of the jump, nor is it affected by the radius of the disk or the thickness at the edge of a flat disk. Despite the simplicity of the present approach, the predicted jump location shows surprisingly close agreement with existing numerical results based on a spectral methodology.

We consider two alternatives to determine the jump height and assess the empirical claim of Duchesne *et al.* (2014) concerning the constancy of the Froude number Fr_J based on the jump radius and height, and its independence of the flow rate. The first approach, following Watson and many others, consists of applying a momentum balance across the (infinitely thin) hydraulic jump, yielding (5.3). We demonstrate theoretically that for both uniform and lubrication flows downstream of the jump, the Froude number is indeed constant as Duchesne *et al.* (2014) claim. However, the predicted values in both cases are higher than their measured value. This simultaneously suggests that the discretized momentum balance approach is not adequate, which is not surprising given the finite thickness of the jump for high-viscosity liquids. This brings us to the second alternative, which consists of solving the film (4.4), either directly or by deducing an asymptotic form far from impingement, taking the thickness H_∞ of the film at the edge of the disk as the boundary condition and integrating (upstream) towards the jump location to determine the height. This approach turns out to be the method of choice as it yields close agreement with the measured Froude number for silicon oil (see figure 10). The value

of H_∞ is determined theoretically as a combined static and dynamic contributions as was done for low-viscosity liquids (Wang & Khayat 2018) but turns out to be relatively much smaller for high-viscosity liquids. Finally, the influence of gravity on the film shape in the entire flow domain is assessed (figure 13).

We observe that the self-similar cubic profiles (3.4) and (4.1) are obviously adopted here for their simplicity, and turned out to be consistently accurate in our comparisons with existing numerical results and experiment. The self-similar cubic profile does not satisfy the momentum equation at the disk, which would break the similarity. The accuracy of the profile used here, despite its simplicity, seems to suggest that, in the KP averaging formulation, the effect of gravity or the pressure gradient in general is not significant at the level of thee solid disk where shearing is dominant. On the other hand, a non-self-similar cubic profile would yield a smooth jump as opposed to the presently predicted shock. Building on the earlier work of Bohr *et al.* (1997), Watanabe *et al.* (2003) used a non-self-similar cubic profile: expression (2.20) in their paper. They obtained the system (2.26) of two ordinary differential equations from their averaged momentum and mass conservation equations. The two unknowns were the film thickness $h(r)$ and a shape parameter $\lambda(r)$ related to the profile coefficients in (2.20). A singularity occurs when $h = 0$ or $\lambda = 7/2$, which is not encountered for the flow they sought. In particular, when $\lambda = 7/2$, their equation (2.24*b*) reduces to $h' = -41/2rh^3$ when their relation (2.14) is used. This expression for the slope indicates that, for the singularity to occur, the slope must be necessarily negative, which is practically not the case for the flow they considered. Their solution was sought by imposing the film heights at two locations obtained from experiment. In that case, the slope is positive or at most mildly negative, and the singularity was thus avoided. This is particularly the case in the subcritical region where the film thickness is high. We refer the reader to figures 4 and 5 in Watanabe *et al.* (2003). We also note that λ was always negative.

However, the singularity is not always avoidable. In particular, when the disk radius is sufficiently large, the film thickness at the edge of the disk can be small enough for h' to remain negative downstream of the jump, thus causing the singularity to occur in the subcritical region. See, for instance, figures 1 and 2 in Duchesne *et al.* (2014), and our own figures 12–14. Consequently, although a non-self-similar cubic profile may yield a smooth jump zone, one may still have to deal with the singularity further downstream. In fact, Bohr *et al.* (1993) did encounter the singularity downstream, and attributed its presence to the edge of the disk.

In closing, we highlight the main points that distinguish our method from the main theoretical literature:

Our approach involves the actual physical domain, ranging from the point of impingement to the edge of the disk, as opposed to the domain located between two arbitrarily chosen points as in Bohr *et al.* (1997) and Watanabe *et al.* (2003).

In this regard, our model does not require any degree of empiricism (other than the flow parameters) such as the imposition of the film heights at the boundary(ies) from experiment (Bohr *et al.* 1997; Watanabe *et al.* 2003; Rojas *et al.* 2013).

Given the essential singularity, the domain is clearly separated, at the level of the shock, into a supercritical flow ahead of the jump and a subcritical flow after the jump. Therefore, there is no overlap in the solution domains on the two sides of the shock as in Kasimov (2008).

Both the supercritical and subcritical flows are sought separately as initial-value problems, starting at theoretically determined initial conditions that correspond to the transition point upstream of the jump and the thickness at the edge downstream.

The jump location is precisely identified to coincide with the location of the singularity of the averaged momentum thin-film equation. In other words, the

singularity is inherent to the momentum and not necessarily to the energy equation as in Bhagat *et al.* (2018).

We attribute the emergence of the jump as the result of the balance between gravity and viscosity, at a point where inertia has sufficiently weakened by the mounting friction, coinciding with the location of the singularity, and not somewhere between the two singularities of the averaged momentum equation as Kasimov (2008) suggested.

The jump location (not height) is determined independently of downstream conditions, such as the disk radius and the edge thickness, in agreement with experiment (Brechet & Neda 1999).

The jump height as well as the entire subcritical flow can be sought *a posteriori*, subject to a well-established boundary conditions at the edge of the disk (static and dynamic contributions at the edge).

Finally, we show the conditions where the Froude number based on the jump height and location is independent of the flow rate, in agreement with the measurements of Duchesne *et al.* (2014).

In conclusion, we demonstrate the crucial role of gravity and its influence on the emergence of the circular hydraulic jump for liquids of relatively large viscosity. We propose a simple and complete theoretical model to predict the location of the jump as well as the flow in the entire domain.

Acknowledgements

The financial support of the Natural Sciences and Engineering Council of Canada is gratefully acknowledged. R.E.K. would like to acknowledge the helpful discussions he had with Professor E. Benilov during his stay at the University of Limerick.

REFERENCES

AVEDISIAN, C. T. & ZHAO, Z. 2000 The circular hydraulic jump in low gravity. *Proc. R. Soc. Lond.* A **456**, 2127–2151.

BAONGA, J. B., GUALOUS, H. L. & IMBERT, M. 2006 Experimental study of hydrodynamic and heat transfer of free liquid jet impinging a flat circular heated disk. *Appl. Therm. Engng* **26**, 1125–1138.

BENILOV, E. S. 2015 Hydraulic jumps in a shallow flow down a slightly inclined substrate. *J. Fluid Mech.* **782**, 5–24.

BHAGAT, R. K., JHA, N. K., LINDEN, P. F. & WILSON, D. I. 2018 On the origin of the circular hydraulic jump in a thin liquid film. *J. Fluid Mech.* **851**, R5.

BOHR, T., DIMON, P. & PUTZKARADZE, V. 1993 Shallow-water approach to the circular hydraulic jump. *J. Fluid Mech.* **254**, 635–648.

BOHR, T., ELLEGAARD, C., HANSEN, A. E. & HAANING, A. 1996 Hydraulic jumps, flow separation and wave breaking: an experimental study. *Physica* B **228**, 1–10.

BOHR, T., PUTKARADZE, V. & WATANABE, S. 1997 Averaging theory for the structure of hydraulic jumps and separation in laminar free-surface flows. *Phys. Rev. Lett.* **79**, 1038–1041.

BRECHET, Y. & NEDA, Z. 1999 On the circular hydraulic jump. *Am. J. Phys.* **67**, 723–731.

BUSH, J. W. M. & ARISTOFF, J. M. 2003 The influence of surface tension on the circular hydraulic jump. *J. Fluid Mech.* **489**, 229–238.

BUSH, J. W. M., ARISTOFF, J. M. & HOSOI, A. E. 2006 An experimental investigation of the stability of the circular hydraulic jump. *J. Fluid Mech.* **558**, 33–52.

CRAIK, A., LATHAM, R., FAWKES, M. & GIBBON, P. 1981 The circular hydraulic jump. *J. Fluid Mech.* **112**, 347–362.

Diversified Enterprises 2009 Surface Energy Data for PDMS (Polydimethylsiloxane) http://www.accudynetest.com/polymer_surface_data/polydimethylsiloxane.pdf.

Dressaire, E., Courbin, L., Crest, J. & Stone, H. A. 2010 Inertia dominated thin-film flows over microdecorated surfaces. *Phys. Fluids* **22**, 073602.

Duchesne, A., Lebon, L. & Limat, L. 2014 Constant Froude number in a circular hydraulic jump and its implication on the jump radius selection. *Europhys. Lett.* **107**, 54002.

Ellegaard, C., Hansen, A., Haaning, A., Hansen, K. & Bohr, T. 1996 Experimental results on flow separation and transitions in the circular hydraulic jump. *Phys. Scr.* **T67**, 105–110.

Ellegaard, C., Hansen, A. E., Haaning, A., Marcussen, A., Bohr, T., Hansen, J. L. & Watanabe, S. 1998 Creating corners in kitchen sink flows. *Nature* **392**, 767–768.

Ellegaard, C, Hansen, A. E., Haaning, A., Hansen, K., Marcussen, A., Bohr, T., Hansen, J. L. & Watanabe, S. 1999 Polygonal hydraulic jumps. *Nonlinearity* **12**, 1–7.

Hansen, S. H., Horluck, S., Zauner, D., Dimon, P., Ellegaard, C. & Creagh, S. C. 1997 Geometric orbits of surface waves from a circular hydraulic jump. *Phys. Rev.* E **55**, 7048–7061.

Higuera, F. J. 1994 The hydraulic jump in a viscous laminar flow. *J. Fluid Mech.* **274**, 69–92.

Kasimov, A. R. 2008 A stationary circular hydraulic jump, the limits of its existence and its gasdynamic analogue. *J. Fluid Mech.* **601**, 189–198.

Kate, R. P., Das, P. K. & Chakraborty, S. 2007 Hydraulic jumps due to oblique impingement of circular liquid jets on a flat horizontal surface. *J. Fluid Mech.* **573**, 247–263.

Khayat, R. E. 2016 Impinging planar jet flow and hydraulic jump on a horizontal surface with slip. *J. Fluid Mech.* **808**, 258–289.

Khayat, R. E. & Kim, K. 2006 Thin-film flow of a viscoelastic fluid on an axisymmetric substrate of arbitrary shape. *J. Fluid Mech.* **552**, 37–71.

Lienhard, J. 2006 Heat transfer by impingement of circular free-surface liquid jets. In *18th National & 7th ISHMT-ASME Heat and Mass Transfer Conference*, pp. 1–17. IIT.

Liu, X. & Lienhard, J. 1993 The hydraulic jump in circular jet impingement and in other thin liquid films. *Exp. Fluids* **15**, 108–116.

Liu, X., Gabour, L. A. & Lienhard, J. 1993 Stagnation-point heat transfer during impingement of laminar liquid jets: analysis including surface tension. *Trans. ASME J. Heat Transfer* **115**, 99–105.

Lubarda, V. & Talke, K. A. 2011 Analysis of the equilibrium droplet shape based on an ellipsoidal droplet Model. *Langmuir* **27**, 10705–10713.

Mohajer, B. & Li, R. 2015 Circular hydraulic jump on finite surfaces with capillary limit. *Phys. Fluids* **27**, 117102.

Ozar, B., Cetegen, B. M. & Faghri, A. 2003 Experiments on the flow of a thin liquid film over a horizontal stationary and rotating disk surface. *Exp. Fluids* **34**, 556–565.

Passandideh-Fard, M., Teymourtash, A. R. & Khavari, M. 2011 Numerical study of circular hydraulic jump using volume-of-fluid method. *Trans. ASME J. Fluids Engng* **133** (1), 011401.

Prince, J. F., Maynes, D. & Crockett, J. 2012 Analysis of laminar jet impingement and hydraulic jump on a horizontal surface with slip. *Phys. Fluids* **24**, 102103.

Rao, A. & Arakeri, J. H. 1998 Integral analysis applied to radial film flows. *Intl J. Heat Mass Transfer* **41**, 275–2767.

Rayleigh, Lord 1914 On the theory of long waves and bores. *Proc. R. Soc. Lond.* A **90** (619), 324–328.

Rojas, N., Argentina, M. & Tirapegui, E. 2010 Inertial lubrication theory. *Phys. Rev. Lett.* **104**, 187801-4.

Rojas, N., Argentina, M. & Tirapegui, E. 2013 A progressive correction to the circular hydraulic jump scaling. *Phys. Fluids* **25**, 042105.

Rojas, N. & Tirapegui, E. 2015 Harmonic solutions for polygonal hydraulic jumps in thin fluid films. *J. Fluid Mech.* **780**, 99–119.

Stevens, J. & Webb, B. W. 1992 Measurements of the free surface flow structure under an impinging, free liquid jet. *Trans. ASME J. Heat Transfer* **114**, 79–84.

Schlichtling, H. 2000 *Boundary-layer Theory*, 8th edn. Springer.

TANI, I. 1949 Water Jump in the Boundary Layer. *J. Phys. Soc. Japan* **4**, 212–215.

VICENTE, C. M. S., ANDRE, P. S. & FERREIRA, R. A. S. 2012 Simple measurement of surface free energy using a web cam. *Rev. Brasil. Ens. Fisica* **34**, 3312,1–5.

WANG, Y. & KHAYAT, R. E. 2018 Impinging jet flow and hydraulic jump on a rotating disk. *J. Fluid Mech.* **839**, 525–560.

WATANABE, S., PUTKARADZE, V. & BOHR, T. 2003 Integral methods for shallow free-surface flows with separation. *J. Fluid Mech.* **480**, 233–265.

WATSON, E. 1964 The spread of a liquid jet over a horizontal plane. *J. Fluid Mech.* **20**, 481–499.

WHITE, F. 2006 *Fundamentals of Fluid Mechanics*. McGraw-Hill.

YANG, S. & CHEN, C. 1992 Laminar film condensation on a finite-size horizontal plate with suction at the wall. *Appl. Math. Model.* **16**, 325–329.

YANG, Y., CHEN, C. & HSU, P. 1997 Laminar film condensation on a finite-size wavy disk. *Appl. Math. Model.* **21**, 139–144.

ZHAO, J. & KHAYAT, R. E. 2008 Spread of a non-Newtonian liquid jet over a horizontal plate. *J. Fluid Mech.* **613**, 411–443.